Compact Prism Assembly for Slit-less Spectroscopy Capability in Roman Space Telescope Wide Field Instrument

Bente H. Eegholm[1,*], Catherine T. Marx[1], Victor J. Chambers[1], Jenny Chu[2], Guangjun Gao[1], Margaret Z. Dominguez[1], John P. Lehan[1], John Hagopian[3], Qian Gong[1], Laurie Seide[4], Evan Bray[5], Charles He[6], Jessica B. Patel[1], Manuel A. Quijada[1], Elliot Malumuth[1], Peter Morey[6], Martina Atanassova[4], Esben Jepsen[4], Jason Krom[4], Brian Kittle[5], Christopher Choi[5], Jonathan Salem[7], Linette D. Kolos[1], Hume L. Peabody[1], James Lyons[1], James A. Corsetti[1], Len Seals[1], Bert A. Pasquale[1], Maxime Rizzo[8], James E. Rhoads[1], Joshua E. Schlieder[1], Sangeeta Malhotra[1], Jeffrey W. Kruk[1], Arthur L. Whipple[8], David A. Content[1]

[1]NASA Goddard Space Flight Center, Greenbelt, MD 20771
[2]McCallie Associates Inc, Goddard Space Flight Center, Greenbelt, MD 20771
[3]Lambda Consulting, LLC, 443 Windsor Farm Road, Harwood, MD 20776
[4]KBR, Goddard Space Flight Center, Greenbelt, MD 20771
[5]Peraton, Inc., Goddard Space Flight Center, Greenbelt, MD 20771
[6]BAE Systems, Goddard Space Flight Center, Greenbelt, MD 20771
[7]NASA John H. Glenn Research Center, Cleveland, OH 44135
[8]Conceptual Analytics, LLC, 8209 Woburn Abbey Road, Glen Dale, MD 20769

ABSTRACT

The Roman Space Telescope (Roman) is a three mirror anastigmat design with a 2.4 m primary mirror. It will be based in the L2 orbit optimized for observations of cosmic expansion using the Wide Field Instrument (WFI) and exoplanet discovery using the Coronagraph Instrument (CGI). The WFI features a 300 megapixel near-infrared detector array providing a field of view >100 times larger than that of the Hubble Space Telescope.

To enable a low-resolution spectroscopy functionality for Roman, a compact Prism Assembly was added, installed in a slot in WFI's element wheel. The Prism Assembly has a 0.75-1.8μm passband enabling a survey of Supernova Type 1a redshifts in the range of 0.2-1.7. It achieves a spectral resolving power of $170 > R > 70$ across the field.

The Prism Assembly had restrictions on size, mass and geometry, and a challenging schedule due to being a late addition to Roman. Despite this, the Prism Assembly is a compact high-performance spectrographic element, implemented as a refractive, all-spherical surfaces, 2-element optical design using S-TIH-1 glass and CaF2. In this paper, we describe the Prism Assembly from design and implementation through alignment, optical performance test and calibration, to delivery for installation in the WFI instrument.

Keywords: optics, spectrometer, optical testing, alignment, CaF_2 calcium fluoride

[*]Bente Hoffmann Eegholm, E-mail: bente.h.eegholm@nasa.gov

1. INTRODUCTION

The 2010 New Worlds, New Horizons Astrophysics Decadal Survey prioritized the Nancy Grace Roman Space Telescope (Roman), at that time known as WFIRST (*Wide Field InfraRed Survey Telescope*), and it followed James Webb Space Telescope (JWST) as NASA's next Astrophysics flagship mission. The science goals of Roman are to provide a deeper understanding of dark energy cosmology and exoplanet information, the accelerated expansion of the universe and large-scale clustering of galaxies and dark matter.

The Roman observatory consists of a telescope with a 2.4 m diameter primary mirror and two instruments, the Wide-Field Instrument (WFI) and the Coronagraph Instrument (CGI), and operates in a libration orbit about the Sun-Earth L2 Lagrange point. The telescope is a three-mirror anastigmat design, partly based on existing hardware and design heritage [1]. Roman's Wide Field channel features a 300 megapixel near-infrared detector array providing a field of 0.8 degrees by 0.4 degrees. This corresponds to a field of view of a factor of >100 larger than the Hubble Space Telescope WFC3-IR camera field of view, and with comparable sensitivity and spatial resolution [2], [3].

In order to enable a low-resolution spectroscopy functionality for Roman, a small Prism Assembly was added to the Roman instrument suite as a sub-assembly to the WFI, located in the WFI Element Wheel. The two instruments, WFI and CGI, share the Primary and Secondary mirrors, after which the input is split up in 2 channels; the WFI channel consists of two flat fold mirrors, followed by a tertiary mirror, which results in a f/8 beam entering the Prism Assembly [4].

As the Prism Assembly was a late add-on to the WFI, the location in one of the slots in the WFI Element Wheel was convenient, as no additional mechanical accommodations or design modifications needed to be made. Figure 1 shows the location of the Prism Assembly in the Element Wheel Assembly (EWA) of the Wide Field Instrument on the Roman Space Telescope. The optical telescope, installed on the Instrument Carrier structure is shown to the left. The relay optics in the Aft Optics Module, consisting of a tertiary mirror and two fold mirrors, and the WFI are shown to the right. The location of the EWA is at the telescope exit pupil, at the entrance of the WFI, with the Prism Assembly shown at the 11 o'clock position. The Prism assembly does not feature a 'spider' mask for the 6 secondary mirror strut locations as it is not necessary to block thermal emission from the telescope.

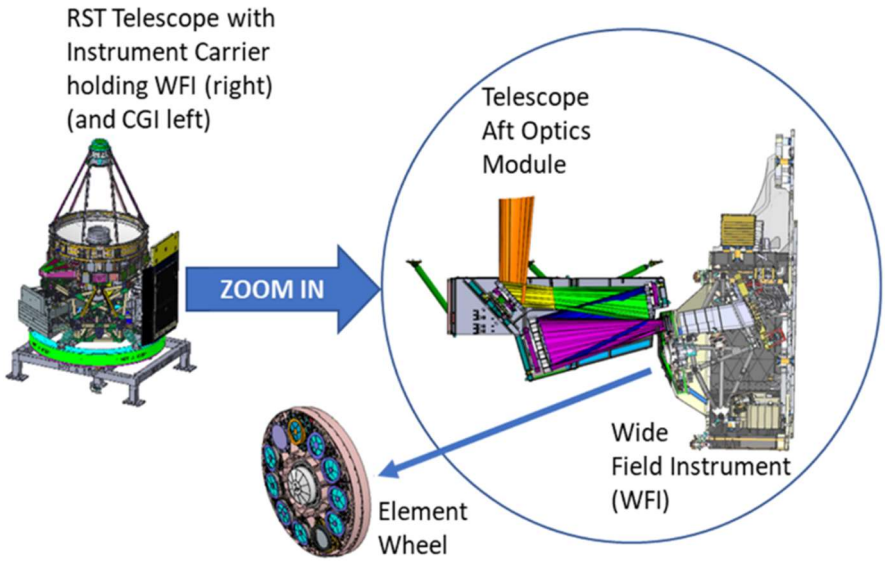

Figure 1. Prism Assembly location in the Element Wheel of the Wide Field Instrument on the Roman Space Telescope. The optical telescope, installed on the Instrument Carrier is shown to the left, the relay optics in the telescope Aft Optics Module and the WFI shown to the right, with indication of the location of the EWA.

The Roman Space Telescope uses multiple independent methods to measure cosmic expansion history and growth of structure. The Prism Assembly provides full field, slit-less spectroscopy in support of Roman's High Latitude Time

Domain Survey (HLTDS) providing information about universe expansion over cosmic history. The role of the Prism Assembly in the study of dark energy is to acquire spectra of Type Ia supernovae; explosion of white dwarfs which exceed threshold mass by accretion. This observation requires measurement of the Silicon lines at 4129 Å and of 6355 Å, along with the lines from Calcium, Sulfur, and Iron. Repeated observations of a supernova survey field during the mission will also build up long exposure times on supernova host galaxies, allowing measurement of their redshifts, primarily using optical emission lines from H alpha (6563 Å) to [OII] (3727 Å) [5] In lieu of adding a Prism assembly to the mission design, additional ground-based spectroscopy was considered as an alternative to cover the desired parameter space. However, it was determined that such an alternative would not be capable of providing the same volume of data in a comparable amount of time.

The dispersion scale and orientation, bandpass edge, throughput, and imaging capability, are key features of the Prism Assembly. Prism yields low dispersion spectra over a wavelength range of 0.75 µm to 1.8 µm, with zero deviation for light near 1550 nm. The Prism passband enables a survey of redshifts in the range from 0.2 to 1.7, with sensitivity to cover the faint afterglow of high-redshift supernovae. The Prism Assembly provides low resolution slit-less spectroscopy over the large field of view with a spectral resolution R>70 for all wavelengths, and R< 170 for wavelengths > 0.8 µm for the center field point.

The light collected by the Roman Space Telescope passes through the EWA before reaching the WFI detector. The EWA is a rotating mechanism which allows the observer to select appropriate filters and elements for specific observations. The WFI element wheel has 11 slots, which hold eight science filters, one dark element, one grating prism (the Grism Assembly), and one Prism Assembly. On orbit the Prism Assembly is dialed in front of the Mosaic Plate Assembly (MPA) 18 segment focal plane array (FPA) with a total of 300 million pixels before science imaging with the Wide Field Instrument begins. An image of the FPA is shown in Figure 2.

WFI also provides attitude correction estimates to the spacecraft based on guide star data collected from the science detectors for fine pointing control of the Observatory. The pointing control requirements are to 10 mas RMS in pitch/yaw. However, because of the instrument design, the guide stars are observed through the same optical element in place for the main observation. This results in a more challenging pointing control for slit-less spectroscopy observations than for direct imaging observations. With the Prism Assembly, guiding is performed using the blue and/or red ends of the stellar spectra that cover about 100 pixels in the dispersion direction.

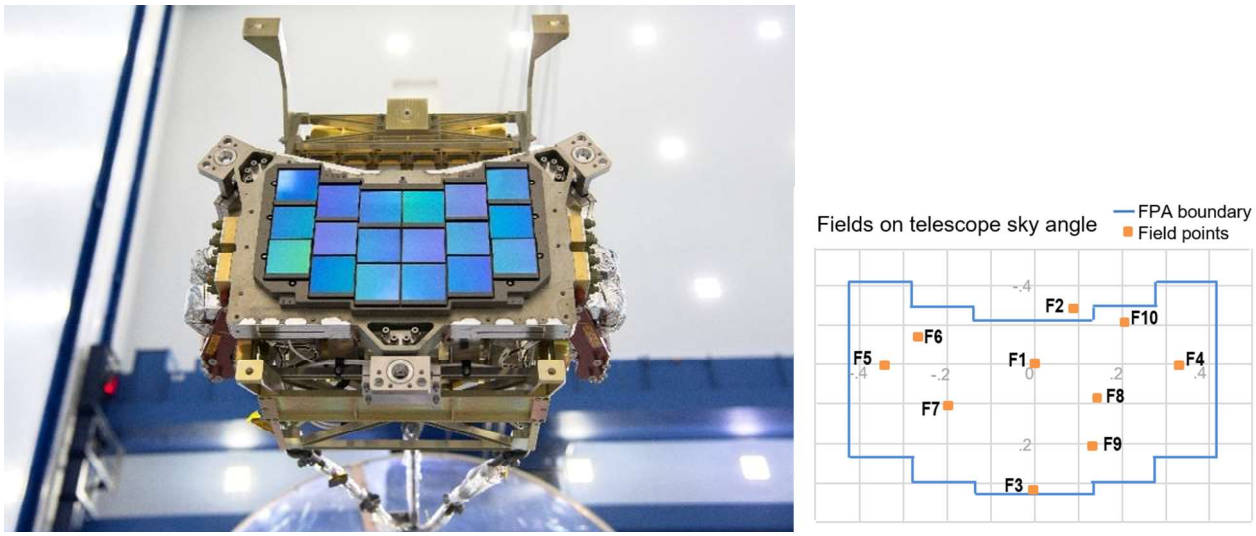

Figure 2. Mosaic plate assembly (MPA) shown left, schematic of Prism test field points location and distribution in the focal plane array shown right.

2. METHODOLOGY

2.1 Design

The Prism design has heritage from earlier incarnations of the mission [6]. There were many design challenges for Prism, besides the envelope constraints. Examples include the f/8 converging beam from the telescope induces aberrations, highly-tilted surfaces, a large field of view and large wavelength range introducing chromatically varying field-dependent aberrations. Furthermore, significant optical imaging design constraints exist for the Prism Assembly, which led to a non-deviating, zero-power system that has to be parfocal with the other elements in the EWA and with the telescope itself. Another challenge for building the Prism was the low on-orbit operating temperature range of 155K-195K, as the design required knowledge of the cryogenic absolute refractive index to $1 \cdot 10^{-5}$.

The placement in the element wheel posed strict limitations on the size, geometry and mass of the Prism Assembly. The physical envelope of the Prism Assembly could be no longer than 86 mm (z-direction), and the optical elements diameter no larger than 119.25 mm. The mass could not exceed 3 kg. These physical restraints were among the drivers for the design solution, and added to the technical challenge of a design covering the entire FOV and the wavelength range. [7].

To achieve the resolving power of the Prism in the space allocated, the wavefront performance deviates from being diffraction-limited over a portion of the field. The Prism is composed of two refractive elements of dissimilar optical materials. A two-element refractive design with all spherical surfaces was favored, since it was considered the least complicated to manufacture, test, integrate and align [8], [9]. Figure 3 shows a diagram of the ray trace through the Prism.

As the Prism was a late addition to the Roman WFI, selecting well-known materials partly mitigated schedule risk. The first element (P1) is made of S-TIH1 glass (manufactured by Ohara), selected to control dispersion. S-TIH1 is a highly-refractive, high-dispersion glass (n=1.71695, v=29.75), chosen because its dispersion yields a resolving power (R), versus wavelength (λ), closest to ideal for supernovae science. The selection of the S-TIH1 glass for P1 was based on heritage design and driven by the Roman science program. The material index of S-TIH1 at cryogenic temperatures had been measured for prior flagship missions at GSFC in the Cryogenic High Accuracy Refraction Measuring System (CHARMS) testbed for an earlier project. [10], [11], [12].

The low dispersion P2 element is installed after the highly dispersive P1 element as a corrector element which allows for integration into the telescope without moving the focal plane. The P2 element is a wedge placed in opposition to the wedged P1 as shown in Figure 3. P2 provides beam steering and balances aberrations caused by P1, and aim the zero beam (chief ray) deviation at the 1550 nm wavelength. The design favored calcium fluoride (CaF_2) as the low-index material (manufactured by Ohara Corp and Hellma Materials) for P2 due to its very low dispersion in the Near-Infrared Region (NIR). CaF_2 has a lower index and lower dispersion (n=1.43479, v=96.66) than S-TIH1. It is a well-known material, yet challenging to source, delicate to handle, manufacture, integrate and bond, especially for the assembly's relatively large 125 mm blank needed. However, alternative materials were not found to satisfy the design goals.

The Prism Assembly length (along the optical axis) is ~80 mm. The largest optical element, P2 (CaF_2) is 119.25 mm in diameter, with a clear aperture of 114.2 mm. The P1 optical element (S-TIH1) is 111.1 mm in diameter, with a clear aperture of 106.0 mm.

The geometry of the Prism optical elements presented both fabrication and mounting challenges since they featured large ten-degree wedges which resulted in relatively thin edges (3-4 mm). These challenges are described below.

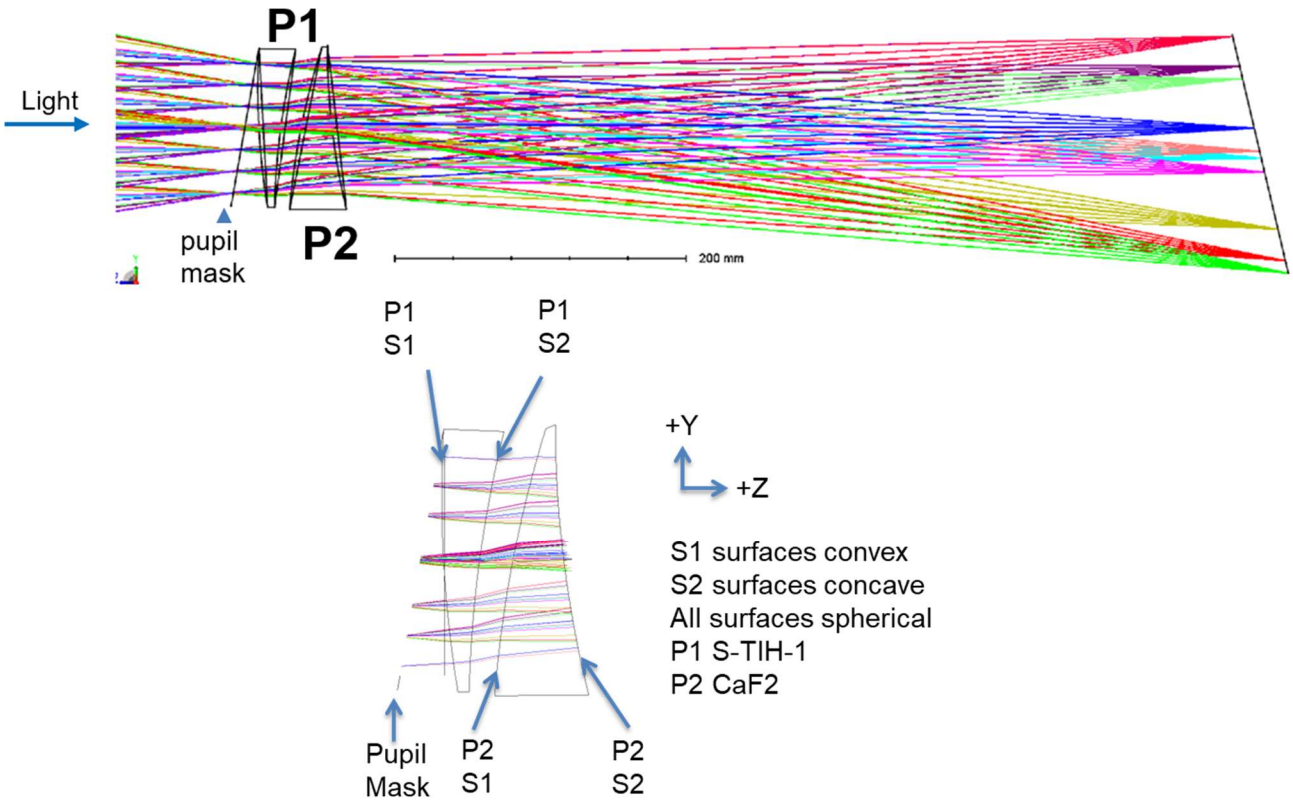

Figure 3. Ray trace of the Roman Prism Assembly. P1 element (left), and P2 element (right). Insert annotates the optical surfaces and materials.

2.2 Implementation

The challenging geometries for P1 and P2, featuring highly wedged shapes between the two spherical surfaces required particular attention during manufacturing, handling, inspection and testing, including custom built mounts for elements testing. See Figure 4.

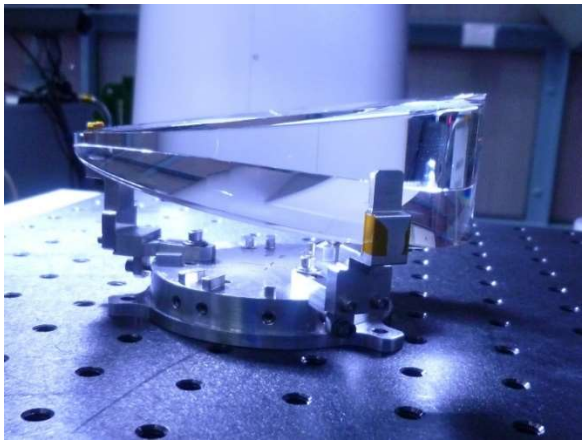

Figure 4. Prism P2 optical element manufactured from CaF_2.

2.3 Calcium Fluoride (CaF_2)

In choosing CaF_2 material for the second wedged prism in the Prism Assembly, it was considered that CaF_2 is a challenging material to work with, especially considering that it represents some of the largest CaF_2 optics that our organization has worked with. For the Prism P2 optic, it was imperative to source large CaF_2 blanks of high homogeneity (refractive index homogeneity <= $1 \cdot 10^{-5}$), low stress birefringence (<10 nm/cm Peak-Valley), and free of grain boundaries and slip planes. The 125 mm +/- 0.2 mm diameter, 45 mm +/- 0.2 mm thick CaF_2 blanks were required to be monocrystalline, required to have high UV grade transmission from visible to near IR. The low stress-birefringence was verified via quantitative mapping (performed at Hinds Instruments). The required crystal orientation was {111}.

Stress birefringence is quantified in [nm/cm], corresponding to the optical path difference per length of material. Stress birefringence, or photo-elastic effect, occurs as a result of pressure or tension. For an optical material, this can be caused by internal or residual stresses. For example, it can be caused by uneven temperature during the annealing process when the internal stress causes an otherwise isotropic material to be anisotropic.

Ordering blanks early in the process was imperative, and sourcing the material from different vendors reduced the technical and schedule risk. The growth time of CaF_2 was taken into account, and since most vendors grow the crystals to order, a lead time of several months was expected. It is possible to search the market for 'remnants' off larger CaF_2 blanks. However, caution should be taken regarding this approach since remnants may be of lower quality that do not meet refractive index homogeneity and stress birefringence requirements. These factors can vary throughout the crystal, such that grain boundaries in the crystal render the blank multi-crystalline.

In addition to ordering CaF2 blanks early, several spare blanks were ordered, since the brittle nature of CaF2 makes the material more prone to breakage during handling and manufacturing, compared to many other commonly used optical materials. At almost any point in the process from shipment through finished optic there is some risk of fracture, and with the long CaF_2 blank lead time, a project can experience serious schedule setback if a spare CaF_2 blank is not readily available.

Upon receiving, thorough inspections of the CaF_2 blanks were conducted to confirm requirements. Inspections included examining the CaF_2 blanks for stress birefringence using crossed polarizers, for example in a microscope with two 90-degree polarizers. However, this is a qualitative method. A quantitative measurement of the stress birefringence was performed using Photo-Elastic Modulation (PEM) technology, where the incoming light is modulated at a high frequency, and a birefringence map of the blank under test is created. The Prism CaF2 blanks underwent this type of test, allowing high accuracy mapping (to < 0.005 nm).[13]. A birefringence map is the result of a photo elastic scan across the entire surface, reading out the birefringence in nm/cm. Figure 5 shows two examples of CaF_2 blanks considered for the Prism P2 element. The top plot shows the stress birefringence map of a high-quality blank which conforms to the requirements. The bottom of Figure 5 is an example of a non-conforming blank with stress birefringence significantly above the requirement, and a low grain boundary seen horizontally in the map and in the adjacent photo of the blank. A low-angle grain boundary may not be a fracture problem, but can be an optics problem. Stress birefringence mapping facilitated selecting the best specimens for use in manufacturing of Prism Flight and Spare optics. It also served as a cross-check to qualify or disqualify other candidate blanks, which could be used in prototyping. (P1 and P2 optical elements were manufactured by Optimax, and QED Optics supplied extra P2 spare).

Another potential CaF_2 issue is the occurrence of slip planes causing slip (deformation), from yielding of the crystal. Slip planes are CaF_2 artifacts associated with stress. The most likely cause being a result of overly aggressive handling during fabrication, or during process steps such as blocking, deblocking, grinding or polishing. However, appearance of slip planes in early stages of fabrication or at blank level indicates a nascent structural defect in the crystal [14].

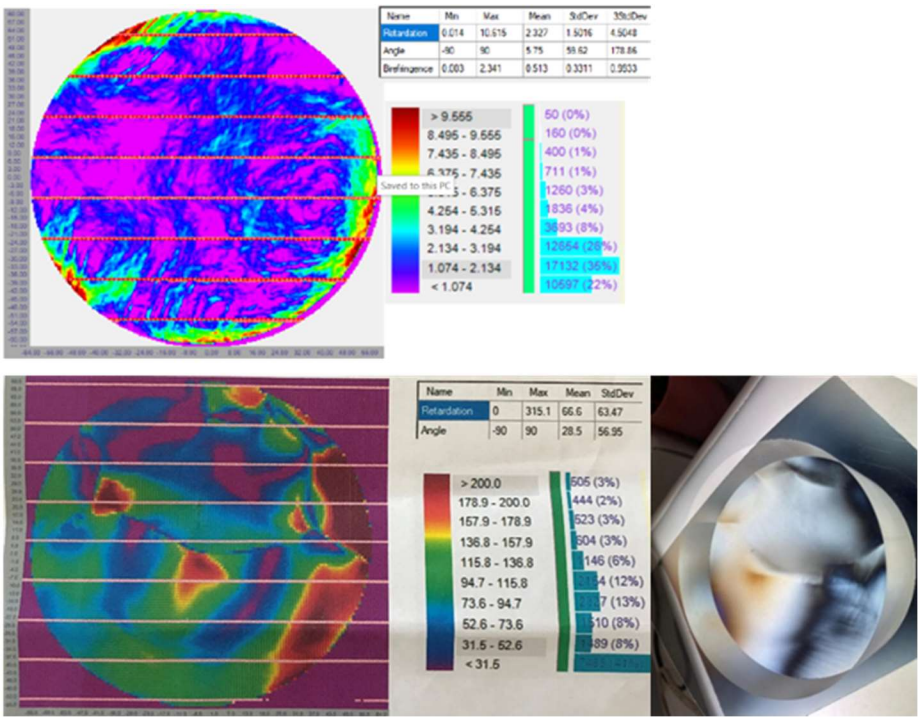

Figure 5. CaF_2 stress birefringence map of high quality CaF_2 blank shown on top: The birefringence is in nm/cm with reference to the color bar to the right of the plot, red indicating the highest, and purple indicating the lowest measured birefringence. Example of stress birefringence map of non-conforming CaF2 blank (bottom): Stress birefringence is much too high. Horizontal low grain boundary is seen in the map (left), also visible on photo (right).

Slip planes can be detected in different ways, at different times in the process. One slip plane was detected via polarization mapping using cross polarizer images at the blank level, indicating a structural defect in the crystal. The slip plane manifested as a square signature. See Figure 6.

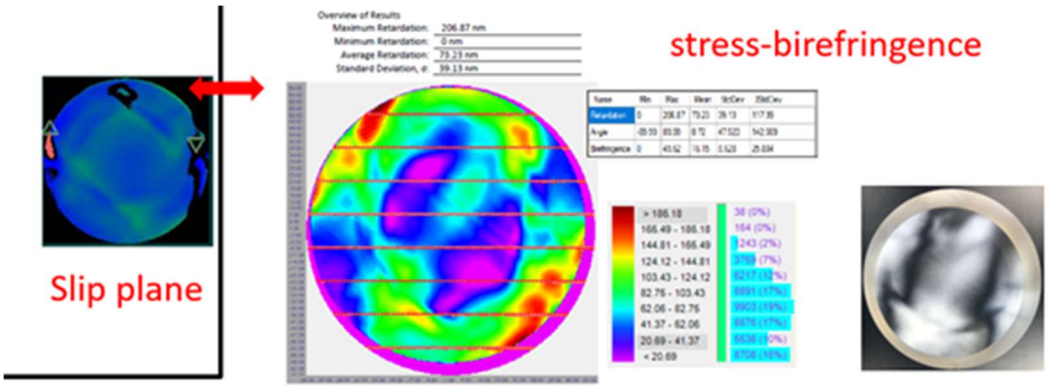

Figure 6. Slip plane detected on CaF_2 blank. Characteristic square signature (left). High stress birefringence indicated in the birefringence map (center). Image (right).

Another slip plane was detected on an early prototype of the P2 optical element during transmitted wavefront interferometry testing with a computer generated hologram (CGH) [15]. This early prototype-was based on a blank which was found to not pass the CaF_2 requirements for the flight optical elements. The slip plane manifested as a square signature in the surface error map. See Figure 7.

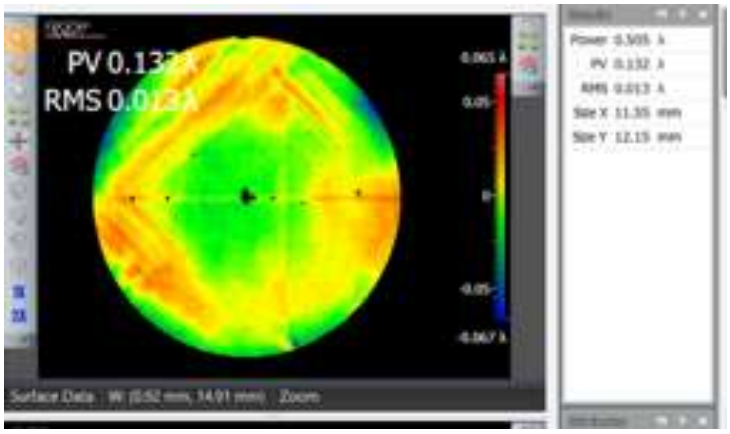

Figure 7. Slip plane on figured optic. Signature from transmitted wavefront error test of an early prototype P2 optic.

Based on the discovery of a slip plane in the early prototype P2 element, all steps of the manufacturing and handling process were re-evaluated with the purpose of identifying process steps, such as blocking, grinding, polishing and deblocking, which might have played a part in the emergence of the slip plane. However, no one step was identified as the sole culprit. However, it is important to note that the manufacturing process for the particular P2 prototype differed from the standard manufacturing process with respect to number of iterations. Since a repolishing of the optical surfaces was needed for this element to achieve the required surface figure, an extra blocking operation as well as a subsequent deblocking operation was needed. It is important to note that the Prism Flight optics did not need these extra process steps. The blanks used for the Flight and Spare optics were selected from a different batch of CaF_2 blanks which had no slip planes, and conformed to all specifications.

CaF_2 cannot withstand large rates of temperature change due to low thermal shock resistance of crystalline materials. The CaF_2 crystals can cleave along their preferred crystal planes when exposed to overly high temperature gradients, especially during cooling. [14]. To minimize the risk of problems due to large temperature gradients for CaF_2, conservative temperature change rates were applied to the Prism optics. These rates were 15 K/hour for heating, and 5 K/hour for cooling. These temperature rate constraints pose restrictions on common processes such as blocking and deblocking, but were also applied for all manufacturing, testing and temperature cycling. Active temperature control was added to the Prism manufacturing process. Furthermore, it was verified that none of the chambers used for optical element temperature cycling as well as for cryogenic optical performance testing of the Prism assembly exceeded theses rates.

In summary, the risks associated with CaF_2 optics were mitigated using both technical and programmatic avenues. The technical risk mitigations included extended characterization of blank inventory, and control of temperature change rates and handling. The programmatic risk mitigations included extended oversight, sourcing extra blanks from different vendors, and sourcing enough CaF_2 blanks to cover two assembly builds and multiple spares.

2.4 Edges

The geometry of the highly-wedged optical elements and limited mass allocations necessitated selection of a radial edge bonding method. To ensure maximum bond strength, the bond area needs to be maximized. It was therefore essential for P1 and P2 to have flawless bevels and impeccable edges. This placed very high surface-quality requirements on the edges of P1 and P2. The bonding allowables were developed based on a perfect surface. During the development phase, bond strength tests were performed, using CaF_2 test coupons manufactured to mimic surface defects. Therefore, the edge

surfaces therefore needed to undergo a final fine polishing step using an abrasive with particle size no larger than one micron.

After an approved blank had been provided to the optics shop, the first order of operation was to generate the edges. Generating the edges was more challenging on CaF_2 than on S-TIH1. The edges of the CaF_2 underwent a thorough inspection before the optical surfaces one (S1) and two (S2) were generated. The inspection was performed on the blocked part, in order to avoid the risk of de-blocking and re-blocking if the edges needed rework. The edges were inspected using a Keyence Digital Microscope VHX7000 with magnification 20x-200x, with 90-degree tilt head to obtain a good view of edges while the optic was held in a support stand. The smoothness of the edges was checked, and reworked if inadequate. Scratches or chips were unacceptable, but the presence of a very limited number of minor sleeks on the edge, which were not endangering the integrity of the part, were accepted.

2.5 Inspection

When inspecting the highly-wedged Prism elements, the tilt-head microscope was used, such that the optical surfaces as well as the optics edges could be examined in the same setting. This required less handling of the finished optic, and less mechanical implements to support the optics standing on its edge, hence reducing the risk of damage during handling. The comprehensive post-polishing incoming inspection program for the Prism optics consisted of weighing and dimensional checks, plus optical microscope inspection of the optical surfaces S1 and S2 for each element, bevels, integral flats, and edges. Furthermore, the optics were inspected for cracks and chips, scratches with/without cracks and chips, pits, sleeks, contaminants (particulate, chemical, etc.), and other unexpected defects. The 45-degree bevels, 0.5mm-1mm wide, between each surface and the edge had to be entirely free of nicks and chips in order to pass inspection.

2.6 Prism alignment features – fiducials and integral flats

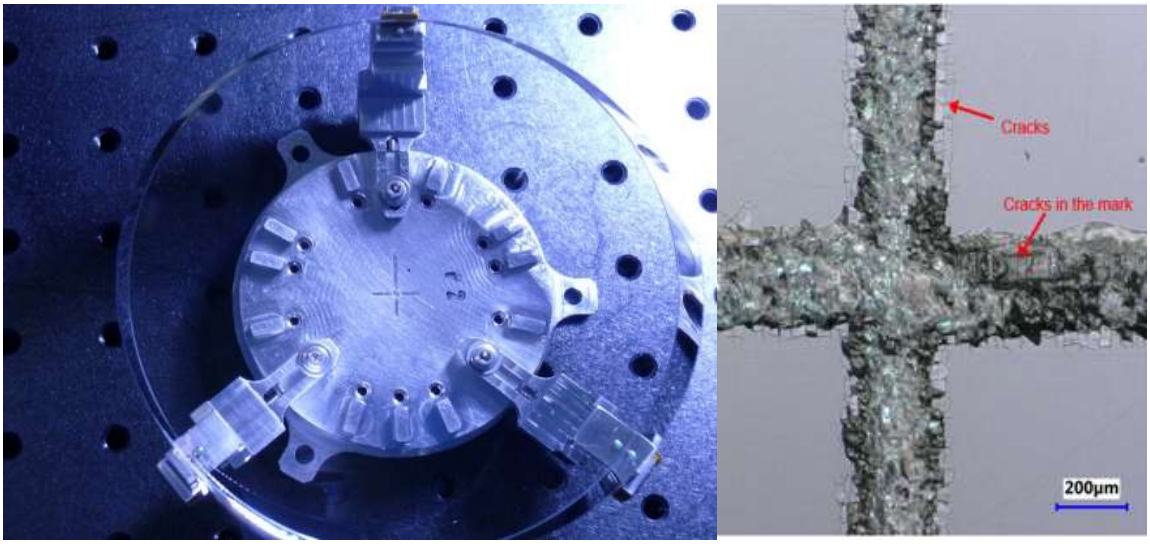

Figure 8. (a) prototype P2 with laser engraved center fiducial. (b) Microscope image of prototype P2's laser engraved center fiducial. Several micro cracks are visible, leading to loose particles.

Fiducials are an important alignment tool for the optical elements. For the Prism prototype P1 and P2 elements, fiducials were laser engraved into the surface. One center fiducial consists of two crossed orthogonal lines, each a few mm long (none of the science field covers the center of the optics), and two additional fiducial markers are 90 degree apart near the edge of the optic, outside the clear aperture. Unfortunately, microscope inspections of the surface showed local damage to the laser engraved area, visible as small chips/cracks, which were found both in the P2 prototype's CaF_2 material, and to a lesser extent P1's S-TIH1 material. It did not look like these had propagated further, judging from a part that had been

thermal cycled and vibration tested. However, it did look like small particles had fallen off and this was assessed to be a contamination risk for the instrument, more than a strength or fracture risk. See Figure 8.

Fiducial application from laser engraving was omitted for flight optics to avoid structural and contamination risks from loose particles. Temporary ink-fiducials were applied as a substitute. These fiducial positions measured in the optical coordinate measuring machine (CMM) prior to alignment and bonding.

Lens alignment also relied on integral flats polished into the edges of both the P1 and P2 optical elements as shown in Figure 9. Figure 9 also includes a photo of the entire P2, with the thin edge in front. The six bond pads are located symmetrically around the lens' Y-axis, which is represented by the symmetry line connecting the thinnest-to-thickest location on the optic.

The integral flats have a flatness of 1/4 wave at 632.8 nm wavelength. They are used to create the part's coordinate system and are positioned 90 degrees apart at the six and three o'clock positions viewed from the P2 S1 surface, and at the twelve and three o'clock positions viewed from the P1 S1 surface. The Y-axis is normal to the six o'clock flat. The twelve and three o'clock flats define the z-axis, and the x-axis is normal to the +Y and +Z axes. Theodolites are used to monitor the flats during alignment, test and bonding.

Figure 9. Photos of P2 optical element after completed manufacturing: Two integral flats are polished into the edges of all optical elements. One flat is shown in the center of the left photo. To the right a photo of the entire P2, thin edge in front.

2.7 Optical performance of individual optical elements

Each element was individually characterized using interferometry with a computer generated hologram (CGH), and optical CMM to determine radius of curvature, before final selection for Flight and Spare elements. The radius of curvature of P1 elements were measured again post coating, with each element in the assembly.

Two complete Prism assemblies were bonded, one Flight Assembly and one Spare Assembly. In addition, one extra P1 spare optical element and three extra P2 spare optical elements were manufactured. The optical performance of each optical element was tested individually as they became available from manufacturing.

CGH were designed and manufactured for each of P1 and P2, [15], at 2 different wavelengths, 1053 nm and 1546 nm, so that testing could take place in two different interferometers to maximize use of time and available metrology equipment. The test of the individual optics took place before any optics were bonded into their cells.

Only the optical elements selected for Flight and Flight Spare were bonded into cells. The selection of the Flight optics P1 and P2 pair, and the Flight Spare P1/P2 pair was based on the measured individual optical performance of every optical element built for the Prism program. Down-selection considered the quality of S1 and S2 surfaces, as well as the edge quality of all the elements.

Ground support equipment (GSE) mounts were developed to hold individual optical elements during qualification optical performance testing. The GSE mounts were equipped with metrology references consisting of laser tracker target nests and optical alignment cubes. The optical element under test was temporarily installed in the GSE mount via cushioned set screws and placed in a Micro-Vu optical CMM to establish the relationship between the element's integral flats and fiducials, the mount's laser tracker targets and optical cubes.

The transmitted wavefront error (TWFE) measurements were performed with an interferometer (1546 nm, Zygo) in double-pass as per Figure 10. The optical element in its LPM was placed on a hexapod to facilitate alignment. A laser tracker was used to guide the P2 positioning via the laser tracker targets placed on the LPM frame. The TWFE and back focal point were measured at the nominal position, and the TWFE was minimized by adjusting the hexapod.

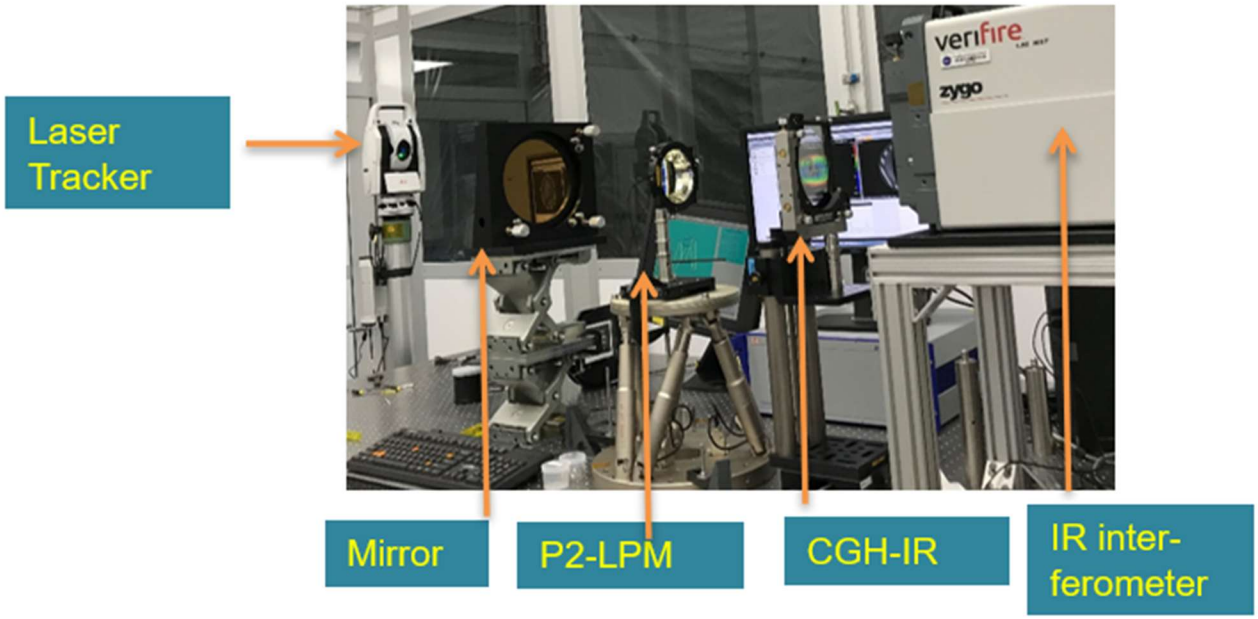

Figure 10. TWFE set up for characterization of individual optical elements.

In addition to the TWFE testing, the radius of curvature was measured for S1 and S2 of the optical elements using a non-contact optical CMM.

To determine which of the P1 and P2 optical elements would be selected and combined for the Flight and Spare assemblies, a thorough down-selection was performed based on the as-built performance results from measurements on the individual optical elements and on model predictions of the performance of each P1-P2 combination in the telescope. The individual TWFE, radius of curvature, mid-spatial frequency content, as well as the quality of optical surface, edges and bevels were also considered.

The four available P2 optical elements were paired up with the three P1's in all permutations. The combined optical wavefront error performance was evaluated in the Zemax model, together with the chief ray deviation, using the as-built data for each optical element. For each possible P1/P2 combination, a Monte Carlo run was performed varying the position of P2 in the mount to meet the WFE requirement and calculate the chief ray deviation. Adjustable parameters included X,

Y (lateral), and R_x. For the combinations with the lowest WFE, a further optimization round was performed to minimize the chief ray deviation. P1 serial number 2 (SN2) paired with P2 serial number 1 (SN1) gave the best combination.

The wavefront error requirement calls for (a contiguous) 90% of the entire field to perform better than 135.1 nm (@1200 nm wavelength, 155 K), i.e., not an average WFE performance metric across the field. The expectation from modelling and experimental work was that the right and left edges would be the most challenging, which was expected due to the focal plane array being longer in X than in Y.

3. PRISM ASSEMBLY AND ALIGNMENT

3.1 Opto-mechanical implementation

The Prism mechanical design features edge bonding of the two elements into individual cells. The assembly strategy was to install each optic in their respective individual cells, then shim the P2 cell at the interface to the P1 cell deck to create the correct relative optical alignment. The P1 deck holds the P2 cell, as well as the P1 mask, and is the reference for all mechanical and optical alignments. See Figure 11.

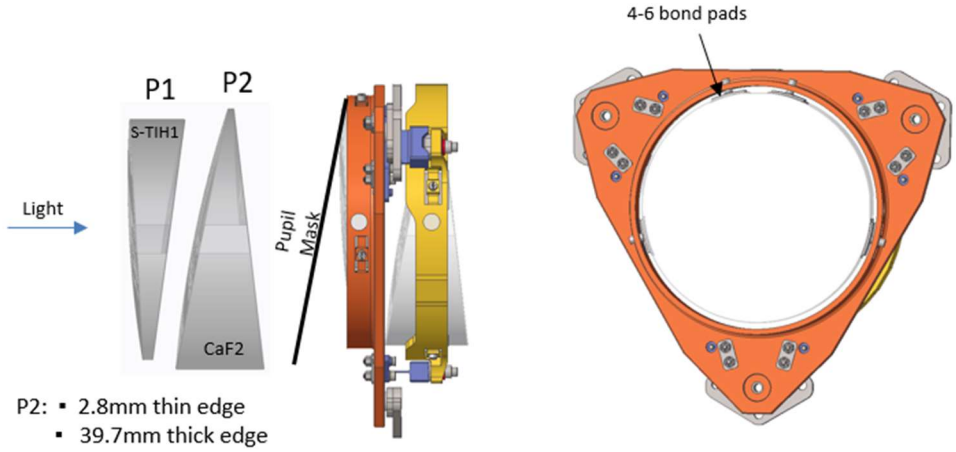

Figure 11. Prism mount. P1 (S-TIH1 element) mounted in the P1 cell to the left (orange), and P2 (CaF2 elements) is mounted in the P2 cell shown to the right of the P1 mount (yellow). The face on view shows the P1 cell seen from the back of P1, with mounting pads ('deck') to hold the P2 cell.

Each of the P1 and P2 optical elements were individually edge-bonded into separate cells. The cell materials were chosen to ensure minimum coefficient of thermal expansion (CTE) mismatch between each optic and its cell. The Prism Assembly would later be mounted to a flexured Titanium interface pad on the Beryllium element wheel.

The P1 optical element was bonded into a titanium cell with four bond pads, and the P2 optical element was bonded into an A286 stainless steel cell with six bond pads, for structural robustness, and redundancy. A Teflon dam was placed to control the bond line shape and thickness.

Figure 12 shows a photo of the Prism Assembly, where the P2 optical element is in view and the P1 optical element is underneath. The bond pads are visible as faint gray circles on the edge of the optic. The completed Prism Assembly measured 207 mm (largest diameter) x 94 mm (long), which was well within the envelope allowed by the Element Wheel.

The Prism P2 cell is attached to the P1 cell with Titanium flexures. Spacing, pointing, decenter, and clocking adjustments of P2 relative to P1 is possible via the kinematic alignment features. The Prism P1/P2 cell interfaces provide adjustment resolution of 30 arc seconds tip/tilt and 12 microns spacing. The Prism Element Wheel interface provides a 1.5 mm centration capability, and 1.5 mm shim capability to adjust spacing and tip/tilt.

An extensive CaF_2 coupon testing program was conducted to determine the best crystal orientation for the P2 optical element and to develop the proper bonding strategy. Several coupons were manufactured for the test program. These included circular disks, 32 mm diameter x 2 mm thick, with faces of all three orientations, {100}, {110}, and {111}, and beams 50 mm long with cross section dimensions of 3 mm x 4 mm and 4 mm x 10 mm. The 3 x 4 mm beams had {100}, {110} or {111} cross section with a 400 grit finish, while the 4 x 10 mm beams were polished but had an unknown orientation.

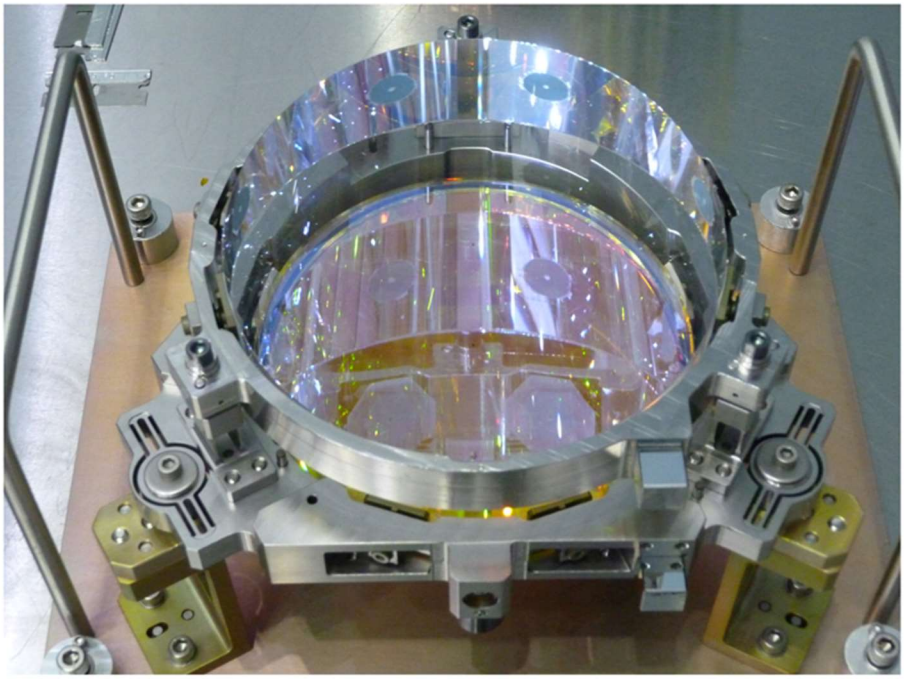

Figure 12. Photo of the Prism Assembly in its (non-flight) transport stand. The P2 element in the A286 Stainless steel cell is facing up. The bond pads are visible around the edge as gray circles.

For {100} polished disks, the strength is about 180 MPa, while for the {110} and {111} faced disks, the strength is about 65 MPa. For ground beams the strength is < 100 MPa, depending on the orientation. The polished beams exhibited a strength of about 115 MPa. Beams are more difficult to polish than disks and are more sensitive to edge damage, which may account for some of the difference.
The conclusion of the coupon testing was that the CaF_2 {111} crystal orientation is the weakest with respect to mechanical properties. However, the {111} face polished better than other orientations, as is confirmed by the material vendor, and is preferred from an optical standpoint. Because the mechanical requirements could be met with a {111} orientation while providing better optical properties, the {111} orientation was used. Details of the mechanical testing can be found in [16], [17].

In order to assess the thermal performance of the optomechanical design, a mechanical model of the Prism Assembly was built, consisting of a S-TIH1 optical element and a CaF_2 optical element, both with flat polished surfaces S1 and S2, as well as cells for each optical element. The optics were bonded in their respective prototype cells and subjected to the flight temperature range of 155 K to 195 K, as well as survival temperature of 137 K, before the figured Prism optics for Flight and Spare were manufactured.

3.2 Alignment of Prism Assembly

The Prism optical element alignment and bonding into cells was based on methodology developed for the Roman Grism [18], [19]. The Prism P1 and P2 optical components were sequentially aligned into their respective mounts, with an optical profiler and two theodolites.

An optic's cell mount was installed on a three-legged stand under the optical profiler where the deck optical cube was calibrated to the coordinate system and features observable by the optical profiler. Additionally, on the optical profiler table, the optical element was placed in an auxiliary, temporary fixture on a hexapod, such that the optical element was inside the cell as shown in Figure 13. The integral flats of the optical element were related to the cell and deck cubes using the theodolites. The hexapod was used to align the optical element into the cell, guided by the theodolite readings. When the alignment process was complete, the bonding adhesive was injected through holes in the cell using a syringe. After the bonds had cured on both P1 and P2, the two units were combined into the Prism Assembly at nominal (design reference) alignment by installing the P2 cell on the deck that holds the P1.

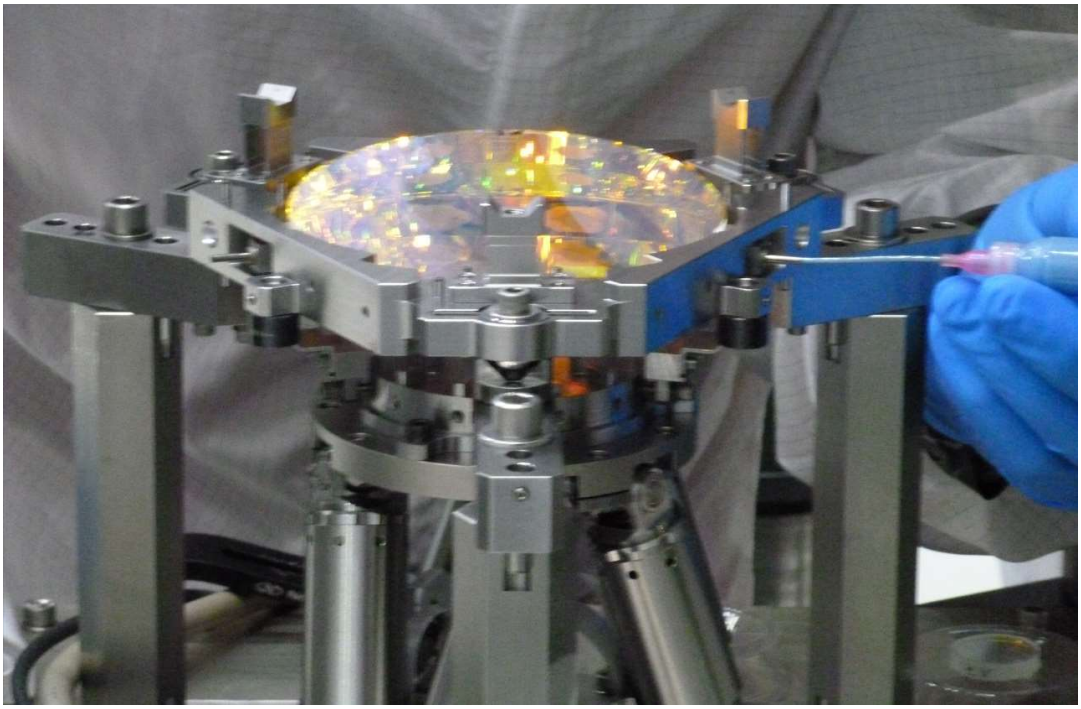

Figure 13. Prism P1 optical element on hexapod for alignment and bonding into cell.

The mount assembly provides a capability to adjust P2 relative to P1 in X, Y, Z and rotation about X (R_x) and Y (R_y), in the local coordinate frame via shimming. The P2 cell adjustability has a limited range (to a maximum of 1.5 mm in each of the X and Y directions). Movement in dZ is an efficient compensator, movement in dY less so, and dY is also mechanically more complicated and riskier to implement. R_y has very limited sensitivity, whereas modeling shows, and alignment tests confirm, that R_x was an efficient compensator for improving optical assembly performance.

The size and shape of the shims needed for the alignment corrections of P2 relative to P1 were determined by ambient interferometer WFE test results and the Zernike composition as a function of field angle. Overall WFE was minimized by balancing Zernike terms on field points on opposite sides of the detector center, where the astigmatism field should have it node. Astigmatism was the dominant field aberration except near the node for all field points. After the WFE test, the measured Zernike terms were plugged into a model of the Prism. This provided the current estimated alignment state relative to the ideal alignment. Shims were then modified to provide the needed adjustment of P2 relative to P1.

The ambient Prism Assembly alignment process using shim optimization was performed over 3 iterations with wavefront error performance of the Prism Assembly measured at ambient in the interferometer between each adjustment. Reducing

the difference between installed and calculated shims helped improve the alignment convergence, which was impacted by shim thickness tolerances. A final re-shim was performed based on the Prism Assembly cryogenic WFE test results.

Figure 14 shows the Prism Assembly with optical axis vertical. P2 visible at the top; pupil mask at the bottom. Simple ink fiducials are in the center of each optic to aid alignment during the element test and integration phases. Nests for Spherically Mounted Retroreflectors (SMR) metrology targets, and alignment cubes on the mounts are used during nominal alignment of the parts.

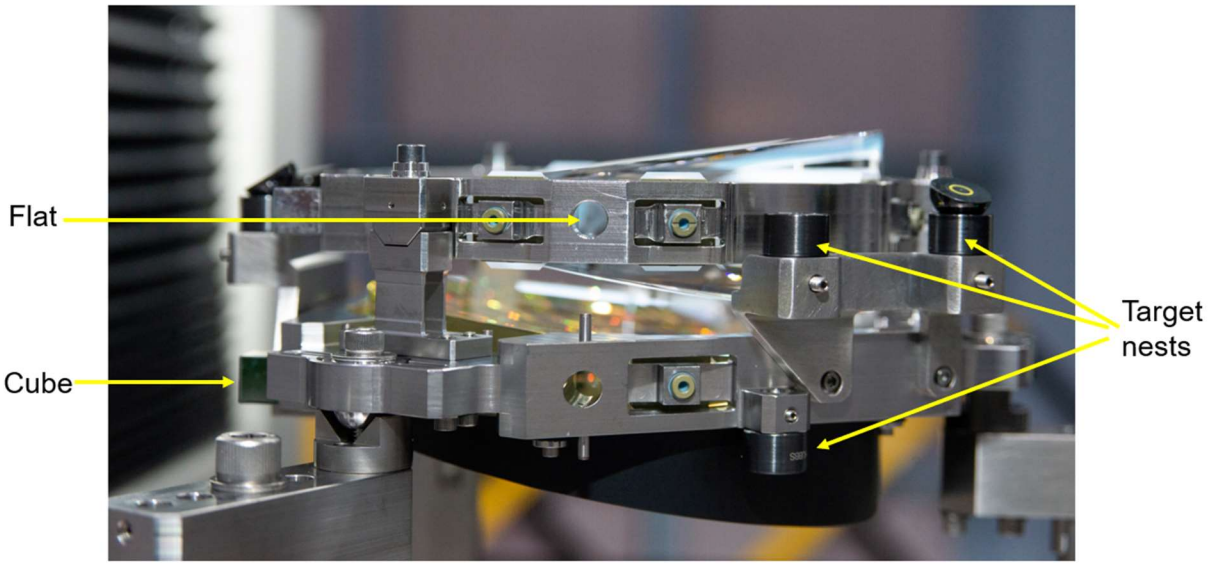

Figure 14. Prism Assembly with optical axis vertical. Some of the cube, flat, and nest metrology aids are pointed out.

4. RESULTS

4.1 Performance testing flow of Prism Assembly

The Prism individual elements and the Prism Assembly were modeled in Zemax, as both an ambient temperature model and a cold as-built model [20]. From the room temperature model, the design values were gradually replaced by as-built values as the Prism was assembled, aligned and tested at ambient temperature and pressure. Cryogenic metrology data was used to mature the Prism's Structural – Thermal – Optical – Performance (STOP) model, which was in turn applied to the Prism's WFE performance model. The optical element positions were optimized within the metrology uncertainty to match the cryogenic WFE testing, by comparing the low order Zernike coefficients. The higher-order Zernike coefficients determined by STOP modeling were adjusted based on the cryogenic interferometric measurements.

The telescope design optical model was used to estimate the end-to-end performance of the entire system (from telescope to Prism Assembly). This was accomplished during the design, test, and integration phases. During the alignment process, the model of the as-fabricated Prism optics was inserted in the Roman Space Telescope optical model to assess the system performance. The Prism Assembly alignment was optimized using the telescope design reference optical model. As per the Roman schedule, Prism Assembly design and development occurred simultaneously with the telescope fabrication and test. Thus, optical performance was modeled using the available as-fabricated values for the telescope mirrors at the time of Prism Assembly development.

Monte Carlo analysis was used to determine the end-to-end system performance of the Prism Assembly inserted in the telescope [20]. As there was not yet any as-built information for the telescope in the Prism alignment, integration and test phase, a pseudo as-built telescope model was used. It was based on the as-fabricated information of the telescope mirrors, alignment errors, adjustment of flight compensators, and on-orbit perturbations. On-orbit, the Secondary Mirror is actuated in five degrees of freedom, and Fold Mirror 1 is actuated in three degrees of freedom. As more of the telescope mirrors (Primary, Secondary, Tertiary, Fold 1, and Fold 2) were completed and tested, the pseudo as-built model was refined, and the Monte Carlo analysis updated. Whereas the Roman Space Telescope offers some adjustability on-orbit via the actuated mirrors as described above, there is no alignment adjustability on orbit for the individual Prism Assembly. There is no refocus adjustment in the Prism mode of the Wide Field Instrument. The focus position is inherited from the Filter mode, where the MPA is actuated in 3-degrees of freedom via a hexapod alignment compensation mechanism.
The process flow chart for the Prism Flight assembly and alignment flow is shown in Figure 15.

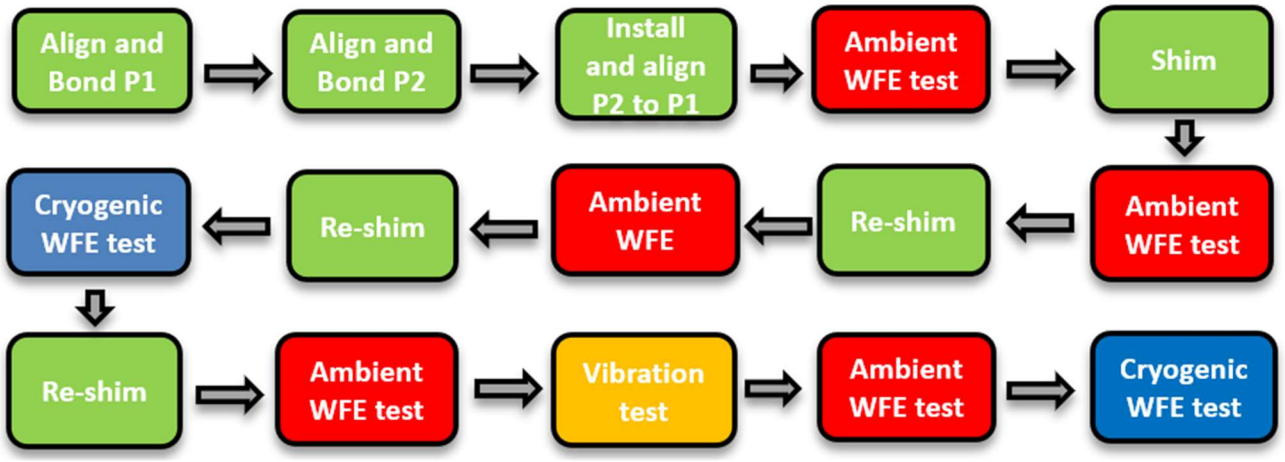

Figure 15. Flow chart for the Prism Flight assembly and alignment flow.
Legend: Box color: Green: Alignment and bonding process. Red: Ambient WFE testing .Blue: Cryogenic WFE testing.

After alignment and bonding of both optical elements P1 and P2, an interferometric WFE test was performed. The result was used to update the model and determine how the shimming under the P2 element cell was to be modified for optimizing assembly alignment. This process was iterated twice before the cryogenic test, after which a final re-shim was determined and implemented. After the final re-shim, the Prism Assembly underwent a vibration test, and a final cryogenic WFE test.

While the Prism Flight Assembly underwent thermal vacuum testing, the Prism Spare Assembly, which had been nominally aligned at ambient, underwent vibration testing. The Prism opto-mechanical design was qualified after successful completion of these tests. The reason for performing the vibration test on the Prism Spare assembly before it was performed on the Prism Flight assembly was to mitigate risk by early opto-mechanical design qualification. The Prism Flight assembly was vibration tested later in the project flow, before its final cold wavefront error performance test. Figure 16 shows the completed Flight Prism Assembly, held in its T-stand used during handling.

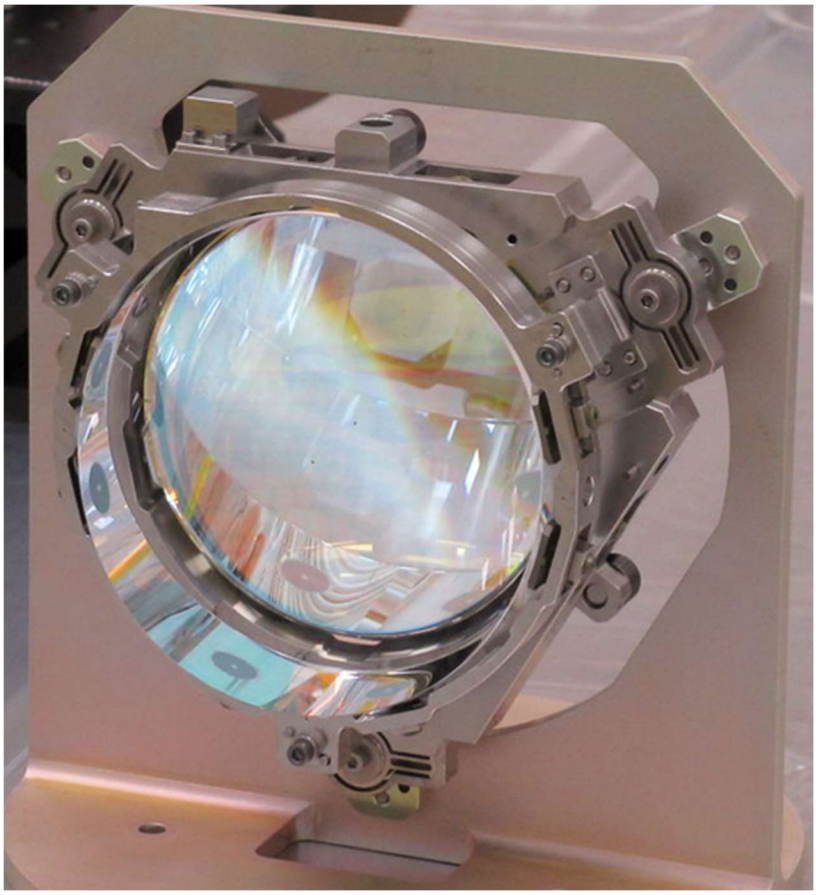

Figure 16. The completed Prism Assembly shown in its T-stand which was used during handling.

4.2 Prism bandpass-coating

The P1 optical element includes a multi-layer bandpass coating (Alluxa). Figure 17 shows the characterization of the multi-layer passband coating at cryogenic and ambient temperatures, and at varying angles of incidence, as a function of wavelength. The P1 element has half the coating layers on S1 and the other half on S2. The filter stops transmission outside the edges of the bandpass. The coating on the front surface, S1, of P1 defines both edges of the bandpass, and the coating on P1's back surface, S2, adds additional blocking in the NIR region. This makes it possible to see through the back surface of P1, which facilitates the bonding process. P2 was not AR coated, as modeling showed that the benefit of coating did not overweigh the risks associated.

The coating, represented by a witness sample coupon, was characterized at GSFC using a Perkin Elmer Lambda 950 spectrophotometer for the measurements at ambient temperature. An Oxford Instruments Optistat CF continuous flow cryostat was added inside the spectrophotometer to obtain coating performance measurements at on-orbit operational cold temperatures. For each, coating performance measurements were obtained as a function of wavelength at varying angles of incidence (AOI) representative of the field points across the wide field. The slight shift to longer wavelengths at increasing temperature is a property of the S-TIH1 substrate-filter interaction [21]. The edge characteristics of the bandpass filter were also measured as well in the Ellipse Testbed described in Section 4.3.

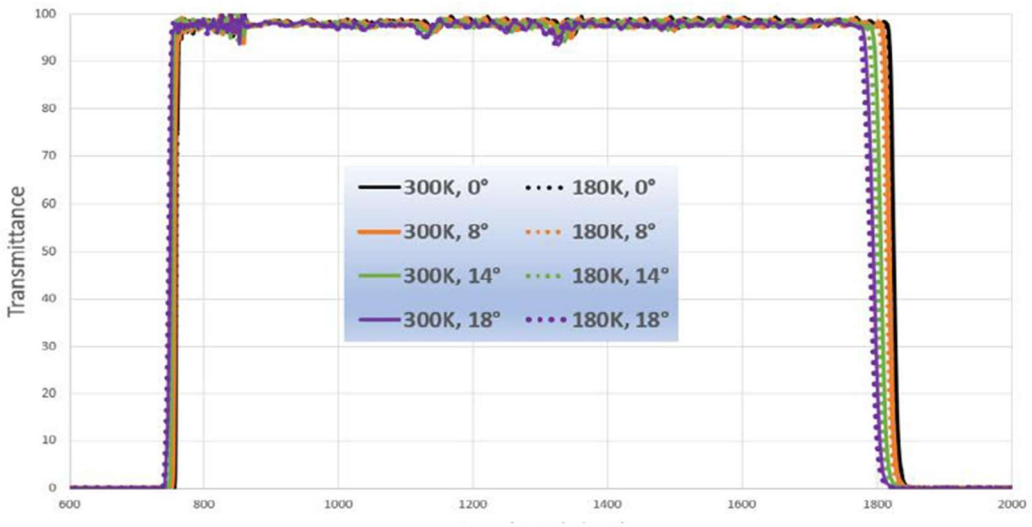

Figure 17. The performance of the multi-layer passband coating on the P1 element at cryogenic and ambient temperatures, and at varying angles of incidence, as a function of wavelength.

4.3 Prism dispersion scale. Prism spectral performance.

The Prism spectral performance was measured in the Ellipse Testbed, which was designed for these measurements for Roman and used to characterize the dispersion scale, dispersion clocking, total throughput, level of ghost imaging, radiometric calibration, and bandpass filter edges of the Prism Assembly [22]. An Argon source calibrated fast Fourier transform (FFT) based Optical Spectral Analyzer was used to calibrate the source wavelengths.

Spectral accuracy and absolute wavelength knowledge were the most challenging tests. Slit-less spectrometers strongly rely on the dispersion scale and bandpass filter edge sharpness to determine absolute λ calibration. The testbed provides a diffraction-limited beam for Prism testing. The light source is a white light laser. A single comb filter spanning 700 nm –2000 nm provides a spectral line series with the desired spacing and bandwidth to perform Prism dispersion scale measurements over the entire spectrum [22]. The layout of the Ellipse Testbed is shown in Figure 18.

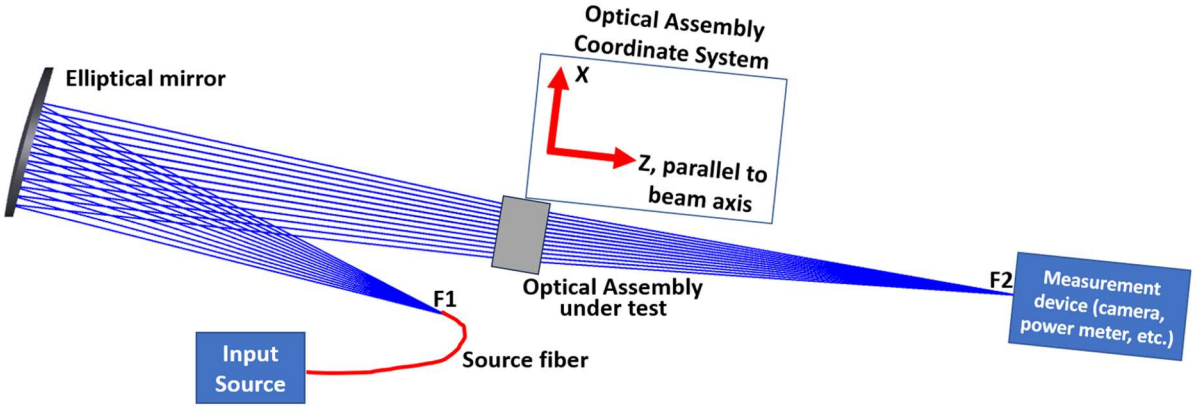

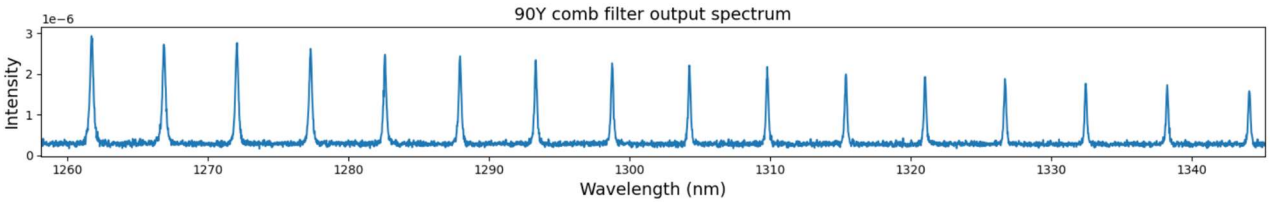

Figure 18. Top: Layout of Ellipse Testbed. Bottom: Accompanying comb filter output spectrum for spectral performance characterization of Prism Assembly. [22].

To accommodate the science goals the required power to resolve adjacent peaks in the spectrum is

$R > 70$ at all wavelengths, and $R < 170$ for all wavelengths $\lambda > 0.8$ µm, across the full field.

The resolving power of Prism is given by $R = \lambda / \Delta\lambda$

where λ is the wavelength, and $\Delta\lambda$ is the greater of 2 pixels, or the full width at half maximum of the optical line-spread function. The pixel size is 10 µm x 10 µm.

This resolving power is achieved for all wavelengths, for all fields. R is directly verified by measurement of the dispersion profile and by showing that the Prism Assembly has a spectral dispersion of between 2 nm/10 µm and 9.5 nm/10 µm for all wavelengths $\lambda > 0.8$ µm across the full field of view. Spectral dispersion versus wavelength measurement is shown in Figure 19.

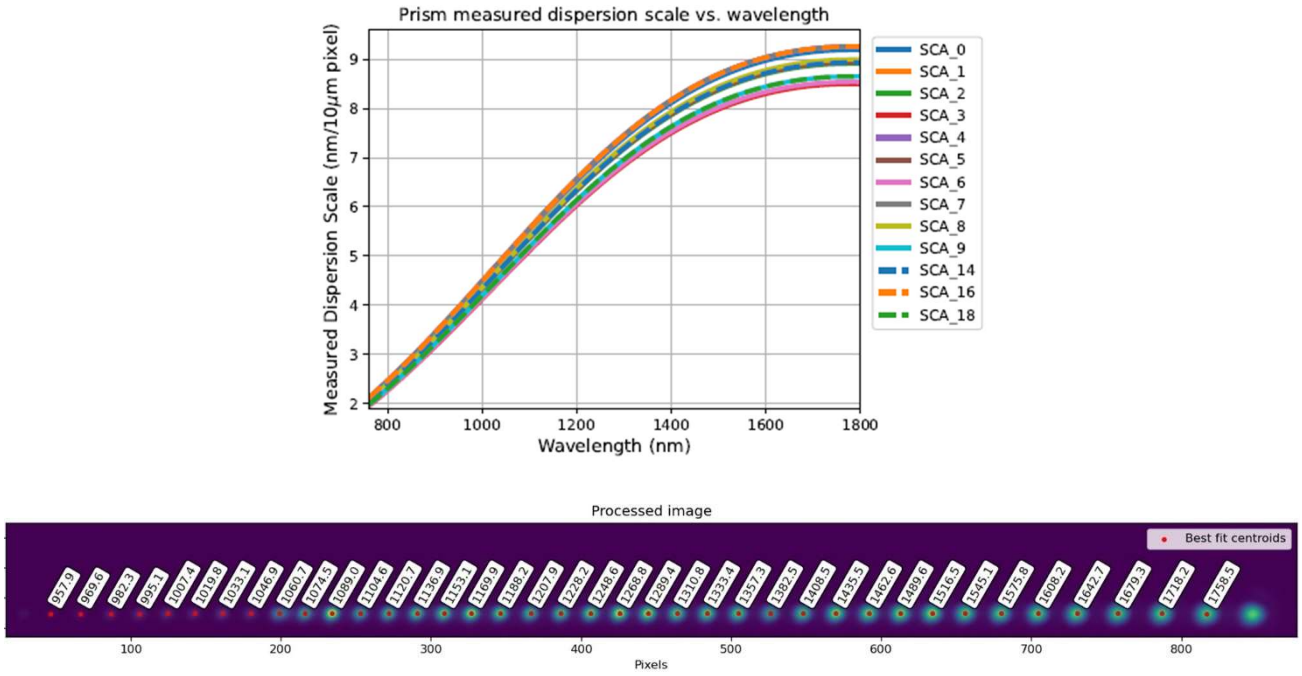

Figure 19. Top: Prism measured dispersion scale vs. wavelength plot for all evaluated field positions. Bottom: An image of the best fit centroid and its location on the sensor for each measured wavelength. [22].

The results from the Ellipse Testbed are the product of many highly-optimized procedures and automation tools developed for acquisition feasibility and speed. Through this test campaign, described in detail in [22], the spectral performance of the Prism Assembly was verified. For completeness, Table 1 lists the findings of the Prism Assembly performance. All

parameters are within the requirements. It should be noted, that for formal verification, the spectral performance is re-measured at cryogenic temperatures later at the Wide Field Instrument level.

The agreement between dispersion scale measurement and model was good, but with a trend of the measured dispersion being slightly lower than expected from the model, yielding a spectral trace 0.7% shorter than expected. This error was low enough that the dispersion was in spec, but not accurate enough for science simulations. Troubleshooting excluded everything other than the refractive index of the Prism P1 material, S-TIH1. CaF_2 was ruled out as a source of error due to its purity and minimal lot-to-lot variation, whereas S-TIH1 is solid solution with small variability. A lesson learned was that relying on a measurement of the refractive index for S-TIH1 from a sample instead of from the same blank as the Prism flight optics added to the uncertainty. During the test phase of the Prism Assembly, the refractive index as a function of wavelength of the as-used S-TIH1 used was estimated and used to improve the fidelity of the as-built Prism model [20].

Raw Ellipse Testbed data were to develop an optical model-based fit. The refractive index was set as a free parameter, but fixed at the lowest wavelength. The resultant indices were interpolated with a 3-term Sellmeier dispersion formula. The updated dispersion allows a single alignment to describe interferometric data and power measurements at 1053 nm & 1546 nm to within error bars [23].

Table 1. Prism spectral performance parameter summary.

Prism parameter	**Measurement**		**Meets spec.?**
Dispersion scale	Shown in Figure 19: 2 nm/pixel < x < 9.5 nm/pixel over the entire wavelength range. Pixel size 10 µm x 10 µm.		Y
Resolving power	The dispersion and WFE requirements for Prism will, when combined with the telescope and MPA, turn into a resolving power; R>70 for all wavelengths, and R< 170 for wavelengths $\lambda > 0.8$ µm for the center field point.		Y
Total throughput	91%, exceeding requirement of 73%. No field dependence		Y
Dispersion clocking	This Prism spectral dispersion is oriented within 0.0053 radians (including the measurement error) of the Y axis.		Y
Ghost imaging level	The area of ghost images is ~1,000 x larger than their parent Point Spread Function (PSF), and the irradiance relative to the parent trace is determined to be of order $\sim 1 \cdot 10^{-7}$. This fulfills with margin the requirement that the integrated power (over twice the spatial size as the primary trace) of ghost artifacts in Prism's optical path < 0.3% of the primary image anywhere on the image plane.		Y
Bandpass filter blue edge and slope	Edge: 761.3 nm Slope: <0.007	Slope: $(\lambda 90 - \lambda 10) / \lambda 50 < 0.007$ Edge at 50%, Full Width Half Maximum (FWHM)	Y
Bandpass filter red edge and slope	1819.7 nm Slope <0.012	Slope: $(\lambda 90 - \lambda 10) / \lambda 50 < 0.03$ Edge at 50%, FWHM	Y

4.4 Prism wavefront error performance

The Flight Prism Assembly underwent thermal vacuum optical performance testing. The optical WFE performance was measured in a cryogenic vacuum chamber in order to test the Prism Assembly as closely to space flight conditions as possible. This also provided for the highest fidelity in the as-built models.

Testing was performed at the nominal operating temperature of 175 K, as well as the low and high operating temperatures of 155K and 195K. The thermal profile of the test included the survival temperature of 137K, which the Prism Assembly must withstand, but at which it is not required to perform optically. The interferometer test wavelength was 1053 nm, and the optical model was used to convert the measured performance to the equivalent performance at 1200 nm, as required for science evaluation purposes [2].

The Prism Assembly underwent two cold optical performance tests. The first was conducted after the 3rd re-shim of the P2 cell which had been performed to optimize the alignment to improve the WFE. The second cold optical performance test was performed after the 4th re-shim was completed, based on the previous measured cold performance.

The cold test was conducted in a cryogenic chamber at the NASA Goddard Space Flight Center (GSFC). The Cryogenic Distortion Measurement Facility (CDMF) is a cryogenic chamber installed on a large optical table. The Prism Assembly and instrumentation was loaded from the top and installed on the baseplate breadboard inside the chamber. An optical window on the right side of the chamber allowed for double-pass interferometry measurements to be acquired with an interferometer that was installed on the optical table outside the chamber. The open CDMF chamber and the location of the Prism and test equipment in the chamber is shown in Figure 20.

The Prism Assembly needs to meet performance requirements over a very large field of view which is 18 degrees by 9 degrees. The thermal-optical performance test setup and equipment did not allow the entire field to be measured simultaneously. Consequently, its wavefront error needed to be measured at several distinct field points. Their selection was based on the modeled performance, and to sample worst-case field point locations impacted by highest measurement error. The center field point is not used on orbit (the physical center field falls in the gap between two of the 18 detector arrays), but it is always included in the measurement series for repeatability and convenience. To accommodate the ten different field points, the Prism Assembly was installed on a motorized gimbal mount inside the chamber. This allowed the Prism Assembly to be moved between measurements to reach the different field points without opening the chamber. The interferometer was installed and aligned outside the cryogenic chamber. Metrology was performed with a laser radar (LR) to monitor physical alignment and determine the Prism Assembly back focal point. A laser tracker (LT) was used for cross-check measurements at ambient conditions with the chamber open.

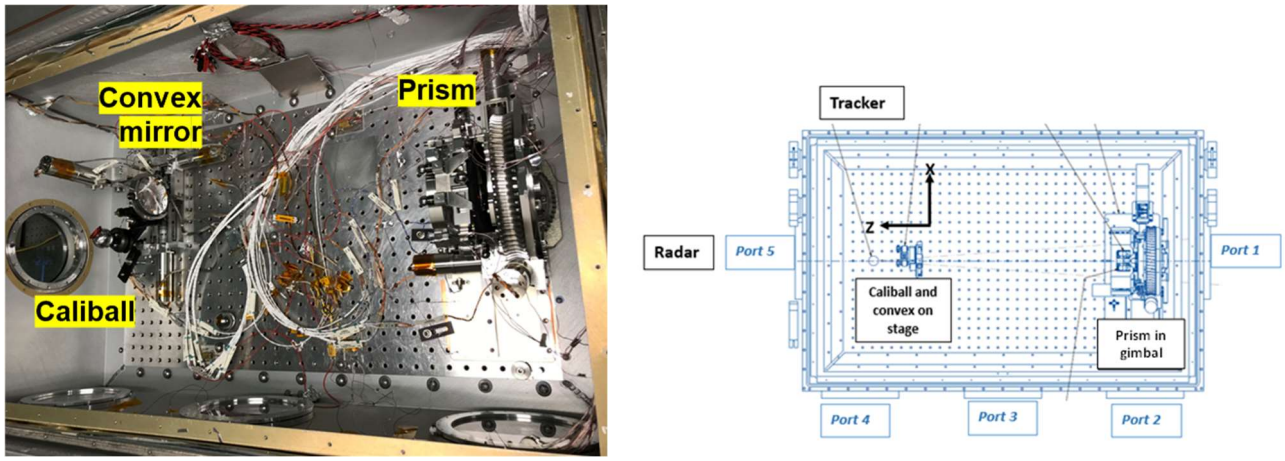

Figure 20. Left: Photo of the CDMF Test Setup with Prism, Calliball, and convex mirror. Right: Top-down view of the CDMF chamber with Laser Tracker and Laser Radar outside.

The laser radar was used to measure the position of targets (tooling balls) when the cryogenic chamber lid was open before and after the cold optical performance test, as well as used to monitor alignment through an auxiliary chamber window during the cold testing (after the chamber lid was closed) [24]. Laser tracker metrology was performed when the chamber lid was open before and after the cold optical performance test, as a supplementary method to track the location of the metrology targets. In particular, it was used to calibrate the gimbal, which did not have a stepper motor. Six tie point targets were placed outside the chamber at positions where they could easily be measured by both the laser tracker and the laser radar. First, the tie point targets were populated with tooling balls, and they (as well as the CaliBall) were measured with the laser radar. Then these targets were swapped out with SMR's, and re-measured using the laser tracker.

The infrared (1053 nm wavelength) 4D interferometer is equipped with a f/6.6 transmission sphere, the closest available to the f/8 provided by the telescope. The high-quality convex spherical retro mirror has a 127 mm radius of curvature and

was placed to the left in the chamber on a motorized 3-axis stage together with a CaliBall, such that the spacing between the Prism pupil mask and the ball was approximately 693.69 mm.

The initial alignment of the setup was performed with the Prism translated out of the beam path, and the interferometer equipped with a transmission flat, used to rough-align the source beam parallel to the chamber baseplate. Fine alignment was performed using a target frame consisting of an empty CGH frame, equipped with four metrology targets, which had previously been characterized in a MicroVu optical CMM.

The Prism Assembly attitude was adjusted with the gimbal for each field point to be measured, and repeated for each temperature. At each position, a measurement was taken with the CaliBall at Prism null in order to determine the back focal point. Afterwards, the convex mirror was positioned at this location using the stage, and a series of WFE measurements were acquired. Insertion of the Prism into the telescope beam should not change the focus of the combination. This was determined by measuring the empty interferometer cavity along with the focal point location with Prism in the beam at all the field angle poses.

The back focal point was determined via laser radar measurements and adjustment of the CaliBall to null power. This was done for each field point measured at each of the cryogenic operating temperatures, 155K, 175K and 195K. The accuracy of the back focal point measurement is dependent on the CDMF combined chamber laser tracker and laser radar metrology accuracy of 28 nm RMS. The back focal point shift was determined to be 36.5 mm@155 K, 29.1 mm@175 K, and 27.2 mm @195 K, respectively.

For the wavefront error measurements, the gimbal and stage positions were adjusted between each field point measurement for a total of ten field points measured, as shown in Figure 2. Per the Prism optical model, the worst-performing field points were predicted to be at the left and right edges of the field of view, since the focal plane array width is larger than its height. Therefore, the field points F4 and F5 were chosen to be as far to each of the sides of the field as physically possible with the maximum gimbal movement.

The Prism Cryovac#2 test, also performed in the CDMF chamber, indicated that the fourth re-shim performed after Cryovac#1, and before the Prism vibration test, had improved the WFE performance adequately over the required 90% of the field. The WFE performance was measured at the nominal operating temperature 175K, as well as the low and high end of the operating temperature range, 155K and 195K. The test was performed over ten field points at 175K, and at 5 field points at the temperatures 155K and 195K. The WFE measurements were passed through a CDMF testing optical model and the resultant prism inserted into the telescope model. The estimated performance in the telescope, reported at 1200 nm, are tabulated per field point and per temperature in Table 2.

The WFE compliance is evaluated based on the overall worst performing field point at the most challenging temperature, 155K, which is F4 at 133.5 nm. The evaluation is not on an average performance over the entire field.

Table 2. Measured WFE at the operating temperature range (reported at 1200nm).

WFE 1200nm	**F1**	**F2**	**F3**	**F4**	**F5**	**F6**	**F7**	**F8**	**F9**	**F10**
[K]	[nm]	[nm]	[nm]	[nm]	[nm]	[nm]	[nm]	[nm]	[nm]	[nm]
155	55.0	62.5	111.0	133.5	119.7					
175	52.2	63.8	105.5	129.4	114.4	77.0	71.7	86.0	110.2	79.2
195	56.6	69.7	105.1	128.1	113.7					

Figure 21 shows Prism Assembly WFE performance in the telescope at 175 K, reported at 1200 nm, based on the cryogenic vacuum test results. The wavefront error at all field points across the Sensor Chip Array are within specification.

The WFE of all 10 measured field points at 175 K were under 135.1 nm with margin. The measurements confirmed that the worst performing measured field points are F4 and F5. F4 is the worst (129.4 nm), followed by F5 (114.4 nm), also with margin. However, F4 and F5, do not quite reach the 90% FOV boundary due to the gimbal movement limitations.

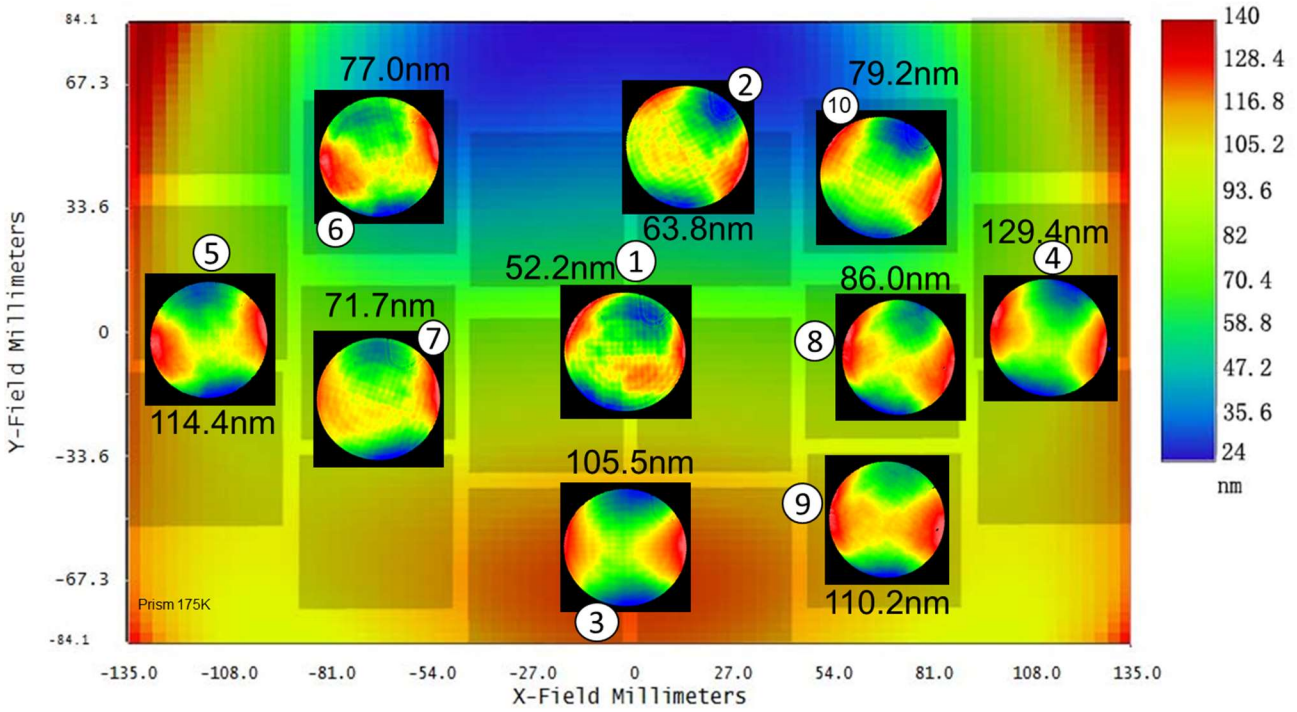

Figure 21. Wavefront error map of the 10 field points measured across the entire field at 175 K. The field point number (white circle insets) show the physical location of each measured field point on the SCA (indicated by the 18 darker colored squares). The numbers in black show the wavefront error (measured @ 1053 nm, reported in the telescope at 1200 nm wavelength.

The performance in the design reference telescope needs to be evaluated over the entire FOV based on the as-built Prism model. Therefore, the optical as-built model is used to calculate the estimated performance at the entire field to report the performance between the measured field points, and beyond 90% of the field.

Figure 22 is a topographic contour map of the as-built Prism Assembly wavefront error at 1200 nm wavelength, using contour lines for every 10 nm to map the wavefront error across the entire FOV. The coldest operating temperature of 155K was the most challenging, and is the temperature for which the compliance evaluation is based. The contour map for 155K shows the performance in the telescope, i.e., the Prism Assembly is installed in the Element Wheel, and the Wide Field Instrument installed in the telescope. The integrated Prism Assembly's performance is further optimized to 135.1 nm by installing the assembly to the EW on a global shim (Rx=0.500°, Ry=-0.280 ° , dz=-.0273 mm), further increasing the margin.

The corresponding number for 175K with the shim is 133.2 nm. The contour lines in the WFE map clearly show the smooth change in performance over the FOV, with most of the area being far below the required WFE. The angular span between the measured fields and the 90% boundary is small, as WFE increases more rapidly closer to the left and right FOV edges.

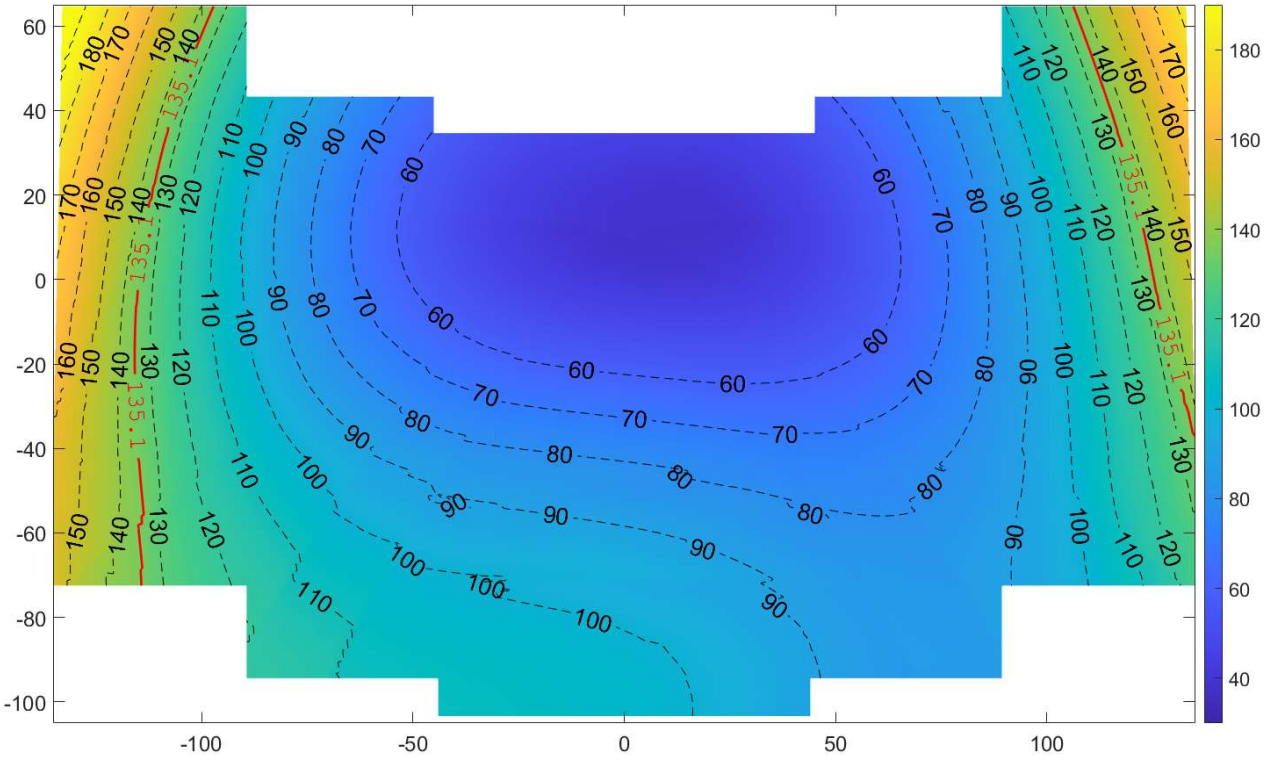

Figure 22. As-built modeled contour map of WFE performance at lowest operating temperature of 155 K over the full field of view. Contour lines shown for every 10 nm WFE, with the boundary of 135.1 nm marked in red.

4.5 Prism WFE budget

The introduction of the Prism Assembly into the Roman WFI optical path must not induce a WFE greater than the 137.5 nm RMS (@ wavelength 1200 nm) without refocusing, because the Roman operations concept does not include refocusing for each individual optical element in the Element Wheel Assembly.

The Prism error budget, shown in Table 3, is estimated to be conservative. The terms in the error budget for the Prism cryogenic vacuum test include the Prism cooldown error from ambient to the coldest 155 K temperature, the contribution from ambient, as well as alignment of Prism in both radial and axial directions. The design residual for the Optical Telescope Assembly (OTA) is included. The Prism is designed to work in the telescope and to minimize the telescope wavefront error plus prism wavefront error across the full field.

Optical coating strain is accounted for in the budget via the cool down term. An End Of Life (EOL) thermal degradation of 2 nm is included in the budget, so that the budget is valid for Roman's five year operation lifetime. To conservatively account for uncertainties in the 175 K model, the budget includes twice the estimated uncertainty, for the most challenging temperature of 155 K.

The uncertainty (19.4 nm), the EOL thermal degradation (2 nm), and the Test-to-Flight thermal condition (15 nm), which are added in RSS (Residual Sum of Squares) to 24.6 nm. This needs to be RSS'ed to the measured WFE (reported at 1200 nm). It should be noted that the 15 nm allocated to the Test-to-Flight thermal condition is considered very conservative. The WFE at the 90% field location is reported in the budget.

Table 3. Prism error budget

Prism Error Budget	WFE with EW shim
Based on worst field at 155 K	[nm]
Prism Total (requirement 137.5 nm)	**137.3**
Prism test at 1200 nm w/OTA design residual	135.1
Radial alignment	Included in measurement
Axial alignment	Included in measurement
Prism cooldown	Included in measurement
Prism ambient contribution	Included in measurement
2 x uncertainty in Measurement–Model at 175K	19.4
End-Of-Life thermal degradation	2.0
Test to Flight thermal condition	15.0

The resulting expected performance for Prism is shown to be 137.3 nm, meeting the 137.5 nm requirement at 90% of the field with a margin of 7.4 nm (RSS).

After testing was completed at the NASA Goddard Space Flight Center, the Prism Assembly was delivered to BAE Systems (formerly Ball Aerospace, partner on Roman Space Telescope Wide Field Instrument) where the integration into the Element Wheel Assembly (see Figure 23) took place. The entire Wide Field Instrument will be installed into the Instrument Carrier (IC) under the telescope at NASA Goddard Space Flight Center, after undergoing thermal vacuum optical performance tests at BAE Systems. The integration of the telescope, science instruments, and spacecraft takes place at NASA Goddard Space Flight Center, forming the Roman Space Telescope Observatory. After testing has been completed at GSFC, Roman will be launched from NASA Kennedy Space Center in Florida.

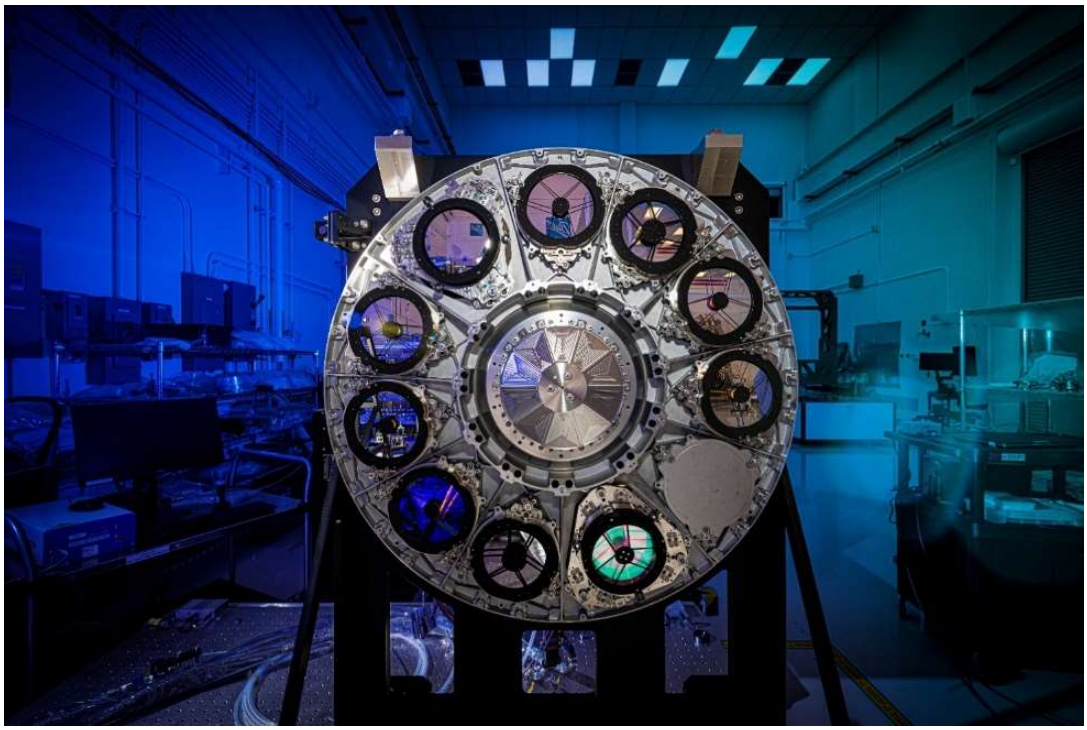

Figure 23. The Element Wheel with the Prism shown to the left of the top element (no spider mask).

5. CONCLUSION

The Prism Flight Assembly has been successfully designed, manufactured, integrated, aligned and tested within requirements levied on it based on Roman Space Telescope science goals. During the development, test and alignment phase, there were several important lessons learned, particularly concerning the early sourcing, use, handling, process control and management of CaF2. These lessons included the need for ample sparing, thorough screening, quantitative testing of CaF2 stress birefringence, strict control of limited temperature change rates, and extremely smooth edge polishing to obtain maximum bonding area and strength. In summary, the risks associated with CaF2 optics were addressed with both technical and programmatic mitigations. Furthermore, continuous optimization of the model with the latest as-built values has been an invaluable tool in achieving compliance to the challenging requirements. The optical performance test results of the individual Prism optical elements, and the quality of their edges, determined the selection of the optical elements for Flight. These were aligned and performance tested as an assembly at ambient and cryogenic operating temperatures. The assembly met requirements and matched model expectations by achieving a 135.1 nm wave front error over at least 90% of the field. Spectral calibration measurements included dispersion scale, dispersion clocking, throughput, bandpass edge characterization and throughput. Their results also matched model expectations, and in some cases exceeded requirements.

6. ACKNOWLEDGEMENTS

The authors would like to gratefully acknowledge the support from NASA's Goddard Space Flight Center under the Roman Space Telescope project for funding this work.

REFERENCES

[1] Bert A. Pasquale, Thomas Casey, Catherine Marx, Guangjun Gao, Nerses Armani, David Content, John Hagopian, Alden Jurling, Clifton Jackson, Alice Liu, Art Whipple, Jacob Murray, "Optical design and predicted performance of the WFIRST phase-b imaging optics assembly and wide field instrument,", Proc. SPIE 10745, Current Developments in Lens Design and Optical Engineering XIX, 107450K (17 September 2018); doi: 10.1117/12.2325859

[2] D. Content, K. Aron, L. Abplanalp, K. Anderson, R. Capps, Z. Chang, J. Dooley, R. Egerman, R. Goullioud, D. Klein, J. Kruk, G. M. Kuan, M. Melton, J. Ruffa, M. Underhill, D. van Buren., "Wide-Field InfraRed Survey Telescope (WFIRST) 2.4-meter mission study." SPIE UV/Optical/IR Space Telescopes and Instruments: Innovative Technologies and Concepts VI. San Diego: SPIE Proceedings, 2013. 7.

[3] R. Hounsell,, D. Scolnic, R. J. Foley, R. Kessler , V. Miranda, A. Avelino , R. C. Bohlin , A. V. Filippenko , J. Frieman3 S. W. Jha, P. L. Kelly, R. P. Kirshner5, K. Mandel , A. Rest, A. G. Riess, S. A. Rodney , and L. Strolger, "Simulations of the WFIRST Supernova Survey and Forecasts of Cosmological Constraints". In: The Astrophysical Journal 867.1 (Oct. 2018), p. 23. doi: 10.3847/1538-4357/aac08b. url: https://dx.doi.org/10.3847/1538-4357/aac08b.

[4] Pasquale, B., Marx, C., Gao, G., Armani, N., Casey, T. "Optical design of the WFIRST Phase A Wide Field Instrument", Proc. SPIE 10590, International Optical Design Conference 2017, 105901Q (27 November 2017).

[5] Joshua E. Schlieder et al. "Science Drivers of the Nancy Grace Roman Space Telescope Grism and Prism". In: Optica Design and Fabrication Congress 2023 (IODC, OFT). Optica Publishing Group, 2023, OM2B.6. url: https://opg.optica.org/abstract.cfm?URI=OFT-2023-OM2B.6.

[6] David Content, et al. "Optical design trade study for the Wide Field Infrared Survey Telescope [WFIRST]", Proc. SPIE, 81460Y (2011).

[7] Bente H. Eegholm, Catherine T. Marx, Victor J. Chambers, Jenny Chu, Jay Voris, Guangjun Gao, John P. Lehan, Laurie L. Seide, Bert A. Pasquale, John G. Hagopian, Peter A. Morey, Qian Gong, Evan Bray, "Prism assembly for Roman Space Telescope Wide Field Instrument slit-less spectroscopy," Proc. SPIE 12180, Space Telescopes and Instrumentation 2022: Optical, Infrared, and Millimeter Wave, 121804X (29 August 2022); https://doi.org/10.1117/12.2633674

[8] Qian Gong et al. "Characterization of Nancy Grace Roman Space Telescope slitless spectrometer (grism)". In: Journal of Astronomical Telescopes, Instruments, and Systems 6.4 (2020), p. 045008. doi: 10.1117/1. JATIS.6.4.045008. url: https://doi.org/10.1117/1.JATIS.6.4.045008.

[9] Guangjun Gao et al. "Nancy Grace Roman Space Telescope Grism and Prism: Optical Design". In: Optica Design and Fabrication Congress 2023 (IODC, OFT). Optica Publishing Group, 2023, OM2B.4. url: https://opg.optica.org/abstract.cfm?URI=OFT-2023-OM2B.4.

[10] D.B. Leviton, B.J. Frey, "Cryogenic, High-Accuracy, Refraction Measuring System – a new facility for cryogenic infrared through far-ultraviolet refractive index measurements," SPIE 5494. 492-504, (2004)

[11] B.J. Frey, D.B. Leviton, "Automation, operation, and data analysis in the cryogenic, high accuracy, refraction measuring system (CHARMS)," SPIE 5904, 212-221, (2005)

[12] Manuel A. Quijada, Douglas B. Leviton, David A. Content, "Cryogenic refractive index and coefficient of thermal expansion of S-TIH1 glass," Proc. SPIE 8863, Cryogenic Optical Systems and Instruments 2013, 886309 (27 September 2013); doi: 10.1117/12.2025510

[13] Wang, B. (2000). Further evaluation of the Exicor birefringence measurement system. Proceedings of SPIE - The International Society for Optical Engineering. 4103. 10.1117/12.403586.

[14] D. Hahn, "Calcium Fluoride and Barium Fluoride Crystals in Optics," Optik&Photonik 4/2014, Wiley-VCH Verlag Gmbh &Co. KGaA Weinheim].

[15] Dominguez, M., Marx, C., Gong, Q., Hagopian, J., Griesmann, U., Burge, J., Kim, D. "Infrared computer-generated holograms: design and application for the WFIRST grism using wavelength-tuning interferometry", Opt. Eng. 57*7), 074105 (2018).

[16] Jonathan Salem, Richard Rogers, and Charles He "Crack propagation in calcium fluoride single crystals", Optical Engineering, 077102-2, July 2023, Vol. 62(7)

[17] Salem J, Murthy P.LN., "Failure location effects on slow crack growth parameter estimates." Int J Ceramic Eng Sci. 2024;6:e10195. https://doi.org/10.1002/ces2.10195

[18] John Hagopian, Joshua L. Berrier, John Chambers, David A. Content, Margaret Z. Dominguez, Qian Gong, Jason Krom, Catherine T. Marx, Joseph C. McMann, Bert A. Pasquale, Laurie Seide, Arthur L. Whipple, and Patrick Williams}, "Alignment and test of the Wide Field Infrared Survey Telescope (WFIRST) Engineering Design Unit (EDU) grism", Optical Engineering + Applications, 2019, url: https://api.semanticscholar.org/CorpusID:203033738

[19] Dominguez, Margaret Z; Eegholm, Bente H; Chambers, Victor J; Fincher, Wesley R; Gao, Guangjun; Gong, Qian; Hagopian, John G; Jepsen, Esben D; Lehan, John P; Marx, Catherine T; Seide, Laurie L, Alignment and wavefront testing results of the Nancy Grace Roman Space Telescope Grism and Prism assemblies. 2023, Optical Fabrication and Testing, Paper# OM2B.2

[20] Guangjun Gao et al. Nancy Grace Roman Space Telescope (RST) Grism and Prism: Flight as-built Models. Gao, Guangjun; Seide, Laurie; Lehan, John; Marx, Catherine; Dominguez, Margaret; Eegholm, Bente; Hagopian, John; Atanassova, Martina; Pasquale, Bert; Gong, Qian; Chambers, Victor J., 2023, Optical Fabrication and Testing, Paper# OM2B.7

[21] Jessica Patel et al. “Spectral characterization of the RST prism assembly bandpass filters”. In: Optical Modeling and Performance Predictions XII. Ed. by Mark A. Kahan. Vol. 12215. International Society for Optics and Photonics. SPIE, 2022, 122150K. doi: 10.1117/12.2633404. url: https://doi.org/10. 1117/12.2633404. 28

[22] E. Bray, M. Batkis, V. J. Chambers, M. Dominguez, B. Eegholm, G. Gao, Q. Gong, W. Halliday, E. Howe, J. Kruk, E. Malumuth, C. Marx, J. Rhoads, M. Rizzo, J. E. Schlieder, L. Seide, E. R. Switzer, J. Voris "Spectral Characterization of the Grism and Prism Slitless Spectrometers for the Nancy Grace Roman Space Telescope, " Journal of Astronomical Telescopes, Instruments, and Systems, Vol. 10, Issue 1, 014003 (February 2024). https://doi.org/10.1117/1.JATIS.10.1.014003

[23] J.P Lehan, E. Bray, J. Voris, C. Marx, B. Eegholm, J. Chambers, Q. Gong, G. Gao, “In-situ Index Determination for the Nancy Grace Roman Space Telescope Wide-field, Slitless, Imaging Prism Spectrometer”, Optica Design and Fabrication Congress, Quebec City, CA, 4-8 June 2023].

[24] T. Hadjimichael, D. Kubalak, A. Slotwinski, P. Davila, B. Eegholm, W. Eichhorn, J. Hayden, E. Mentzell, R. Ohl, G. Scharfstein, and R. Telfer "Cryogenic metrology for the James Webb Space Telescope Integrated Science Instrument Module alignment target fixtures using laser radar through a chamber window", Proc. SPIE 7793, Optical System Alignment, Tolerancing, and Verification IV, 77930B (3 September 2010); https://doi.org/10.1117/12.862693